22-10-2014

# Continuity of mammalian fauna over the last 200,000 y in the Indian subcontinent

Patrick Roberts
*University of Oxford*

Eric Delson
*City University of New York*

Preston Miracle
*University of Cambridge*

Peter Ditchfield
*University of Oxford*

Richard G. Roberts
*University of Wollongong*, rgrob@uow.edu.au

*See next page for additional authors*

# Continuity of mammalian fauna over the last 200,000 y in the Indian subcontinent


## Abstract

Mammalian extinction worldwide during the Late Pleistocene has been a major focus for Quaternary biochronology and paleoecology. These extinctions have been variably attributed to the impacts of climate change and human interference. However, until relatively recently, research has been largely restricted to the Americas, Europe, and Australasia. We present the oldest Middle-Late Pleistocene stratified and numerically dated faunal succession for the Indian subcontinent from the Billasurgam cave complex. Our data demonstrate continuity of 20 of 21 identified mammalian taxa from at least 100,000 y ago to the present, and in some cases up to 200,000 y ago. Comparison of this fossil record to contemporary faunal ranges indicates some geographical redistribution of mammalian taxa within India. We suggest that, although local extirpations occurred, the majority of taxa survived or adapted to substantial ecological pressures in fragmented habitats. Comparison of the Indian record with faunal records from Southeast and Southwest Asia demonstrates the importance of interconnected mosaic habitats to long-term faunal persistence across the Asian tropics. The data presented here have implications for mammalian conservation in India today, where increasing ecological circumscription may leave certain taxa increasingly endangered in the most densely populated region of the world.



## Keywords

Billasurgam, Kurnool, Theropithecus, extinction, conservation, CAS





## Publication Details

Roberts, P., Delson, E., Miracle, P., Ditchfield, P., Roberts, R. G., Jacobs, Z., Blinkhorn, J., Ciochon, R. L., Fleagle, J. G., Frost, S. R., Gilbert, C. C., Gunnell, G. F., Harrison, T., Korisettar, R. & Petraglia, M. D. (2014). Continuity of mammalian fauna over the last 200,000 y in the Indian subcontinent. Proceedings of the National Academy of Sciences of USA, 111 (16), 5848-5853.



## Authors

Patrick Roberts, Eric Delson, Preston Miracle, Peter Ditchfield, Richard G. Roberts, Zenobia Jacobs, James Blinkhorn, Russell L. Ciochon, John G. Fleagle, Stephen R. Frost, Christopher C. Gilbert, Greg F. Gunnell, Terry Harrison, Ravi Korisettar, and Michael D. Petraglia

Biological Sciences: Anthropology, Ecology, Evolution, Atmospheric, & Planetary Sciences

# Continuity of Mammalian Fauna Over the Last 200,000 Years in the Indian Subcontinent

Short title: **Continuity of Indian Pleistocene Mammalian Fauna**

Patrick Roberts[1], Eric Delson[2,3], Preston Miracle[4], Peter Ditchfield[1], Richard G. Roberts[5], Zenobia Jacobs[5], James Blinkhorn[6], Russell L. Ciochon[7], John G. Fleagle[8], Stephen R. Frost[9], Christopher C. Gilbert[10], Gregg F. Gunnell[11], Terry Harrison[12], Ravi Korisettar[13], Michael D. Petraglia[1,14]

[1] School of Archaeology, Research Laboratory for Archaeology and the History of Art, University of Oxford, Dyson Perrins Building, South Parks Road, Oxford OX1 3QY, UK.

[2] Department of Vertebrate Paleontology, American Museum of Natural History, New York, NY 10024, USA.

[3] Department of Anthropology, Lehman College/ City University of New York, Bedford Park Boulevard West, Bronx, NY 10468 USA; and The Graduate Center, City University of New York and New York Consortium in Evolutionary Primatology, New York, NY 10016, USA.

[4] Division of Archaeology, University of Cambridge, Downing Street, Cambridge CB2 3DZ, UK.

[5] Centre for Archaeological Science, School of Earth & Environmental Sciences, University of Wollongong, Wollongong, New South Wales 2522, Australia.

[6] PACEA, Université Bordeaux 1, Bâtiment B 18, Avenue des Facultés, 33405 Talence Cedex, France.

[7] Department of Anthropology and Museum of Natural History, University of Iowa, Iowa City, IA 52242 USA

[8] Anatomical Sciences, School of Medicine, Stony Brook University, Stony Brook, NY 11794-8081 USA.

[9] Department of Anthropology, University of Oregon, Eugene, OR 97132-1218 USA.

[10] Department of Anthropology, Hunter College/City University of New York, 695 Park Avenue, New York, NY 10065 USA; and The Graduate Center, City University of New York and New York Consortium in Evolutionary Primatology, New York, NY 10016, USA.

[11] Division of Fossil Primates; Duke Lemur Center; 1013 Broad Street; Durham, NC 27705 USA; and The Graduate Center, City University of New York and New York Consortium in Evolutionary Primatology, New York, NY 10016, USA.

[12] Center for the Study of Human Origins, Department of Anthropology, New York University, 25 Waverly Place, New York, NY 10003, USA and New York Consortium in Evolutionary Primatology, New York, NY 10016, USA.

[13] Department of History and Archaeology, Karnatak University, Dharwad 580-003, India

[14] Human Origins Program, Smithsonian Institution, Washington, DC, 20560 USA.

correspondence to: Michael D. Petraglia
email: michael.petraglia@rlaha.ox.ac.uk
School of Archaeology, Research Laboratory for Archaeology and the History of Art, University of Oxford, Dyson Perrins Building, South Parks Road, Oxford OX1 3QY, UK
Telephone: +441865 275373

KEYWORDS: Billasurgam, Kurnool, *Theropithecus*, extinction, conservation

*Abstract:*

Mammalian extinction worldwide during the Late Pleistocene has been a major focus for Quaternary biochronology and paleoecology. These extinctions have been variably attributed to the impacts of climate change and human interference. However, until relatively recently, research has been largely restricted to the Americas, Europe, and Australasia. We present the oldest Middle-Late Pleistocene stratified and numerically dated faunal succession for the Indian subcontinent from the Billasurgam cave complex. Our data demonstrate continuity of 20 of 21 identified mammalian taxa from at least 100,000 years ago to the present, and in some cases up to 200,000 years ago. Comparison of this fossil record to contemporary faunal ranges indicates some geographical redistribution of mammalian taxa within India. We suggest that while local extirpations occurred, the majority of taxa survived or adapted to substantial ecological pressures in fragmented habitats. Comparison of the Indian record with faunal records from Southeast and Southwest Asia demonstrates the importance of interconnected mosaic habitats to long-term faunal persistence across the Asian tropics. The data presented here have implications for mammalian conservation in India today, where increasing ecological circumscription may leave certain taxa increasingly endangered in the most densely populated region of the world.

SIGNIFICANCE STATEMENT: Mammalian extinction during the past several hundred thousand years has been a major focus for evolutionary biologists, geologists and archaeologists, often being linked to climate change and human over-hunting. Until relatively recently, study has been largely restricted to the Americas, Europe, and Australasia. We present the oldest well-dated sequence of mammalian faunas for the Indian subcontinent, demonstrating continuity of 20 of 21 identified mammals from at least 100,000 years ago to the present. We suggest that while local extirpations occurred, the majority of taxa survived or adapted to substantial ecological pressures in fragmented habitats. These results complement data from Africa and elsewhere that demonstrates the necessity of a nuanced ecological understanding of such extinctions in different areas of the world.

**\body**

## Introduction

The extinction of many Late Pleistocene mammals has been described as a "major event in recent Earth history" (1). For a long time attention has focused on terrestrial 'mega'-fauna (>44 kg), with 97 of 150 genera becoming extinct worldwide by 10 thousand years ago (ka) (2). Climate change and over-hunting or habitat disruption by humans are typically cited as causes for the widespread disappearance of these mammals, but research in Africa and a growing understanding of fauna–ecosystem interactions suggests that single-factor explanations for faunal extinctions are over simplistic (2−5). Furthermore, the simultaneous disappearance of smaller mammalian taxa in some regions (6), but not in others (3), suggests that Late Pleistocene mammalian population analyses should also consider multiple causes acting on different taxa at a range of spatial and temporal scales, and that wider ecological perspectives should be embraced (1). Securely dated Pleistocene fossil assemblages from less well-documented regions of the world therefore offer considerable potential to further our knowledge about the factors affecting past faunal distributions and diversity.

The Indian subcontinent preserves a mosaic of ecosystems, ranging from tropical rainforests to grassland savannahs and deserts (7). This ecological diversity would have supported a large range of organisms (8), yet little research has been undertaken on Pleistocene mammalian population changes in the region owing to a lack of stratified finds. Indian ecosystems are subject to the influence and strength of the Indian Summer Monsoon (9) and the subcontinent is likely to have been one of the first regions reached by early modern humans leaving Africa in the Late Pleistocene (10, 11), with potential repercussions for mammalian communities. Human impact on mammals in regions beyond India has been much discussed (1, 3), but the influence of modern human arrival on faunal populations in

South Asia remains unknown, as does the possible effect of the ~74 ka Toba volcanic super-eruption (12). The Indian subcontinent therefore presents a critical, but poorly documented, region for investigating faunal responses to climatic, volcanic and anthropogenic-driven change during the Pleistocene. In this paper we report the earliest well dated, stratified Middle–Late Pleistocene faunal sequence from the Indian subcontinent.

## Results and Discussion

### *The stratified faunal sequence*

The Billasurgam cave complex, Kurnool District, Andhra Pradesh (N15°26.153' E7°11.122') (Fig. 1) lies in a semi-arid tropical landscape, with an average annual rainfall of 700 mm. The cave complex consists of an interconnected series of large chambers within Palaeozoic carbonate host rock. Excavations have focused on the thick (>10 m) sequences of Quaternary sediments preserved within the major chambers of Charnel House Cave and Cathedral Cave. Although the abundance of fossils has led to intermittent research and excavation of the Billasurgam caves since the 19$^{th}$ century (13, 14), the faunal sequence has not previously been dated or systematically analysed in order to understand past biodiversity and faunal dynamics. Previous excavations at Billasurgam and in nearby caves reportedly produced Upper Palaeolithic artefacts alongside cut-marked bones (15, 16), but no such evidence has been identified in recent excavations and bone striations and damage have been attributed to animal gnawing (17, 18). The sedimentary sequence within the cave complex is dominated by silt grade siliciclastic deposits (referred to as 'cave earths' by Foote (13)). These are punctuated by occasional layers of coarse breccia related to minor periodic roof collapse. The majority of the sedimentary input to the cave complex has been via surface runoff into a well-developed network of sinkholes. There is also a minor component of wind-blown

material in the sequences near the main entrance. There is no evidence of significant fluvial input or reworking of the sediments.

*Optically Stimulated Luminescence (OSL) dating*

Eight sediment samples were dated by OSL from the Charnel House Cave and Cathedral Cave sequences. The four samples from Charnel House Cave indicate that the sampled deposits are largely dated to between 74 and 57 ka (Fig. 2, SI Appendix Table S10). This complements previous publications of tephra analysis undertaken on the Charnel House Cave sequence that demonstrated the presence of ash shards from the Toba eruption (19) (see Fig. 2). Finds of pottery date the uppermost levels of Charnel House Cave to the Holocene.

OSL dating of the Cathedral Cave sediments indicates deposition between approximately ~210 and 120 ka (Fig. 2, SI Appendix Table S10), with at least 4.5 m of overlying (younger) deposits removed by 19th century excavations (13).

Figure 2 shows the scientific dating results at the two sites and their correlation with Marine Isotope Stages (MIS). The dating confirms that the Billasurgam cave complex represents the oldest Middle-Late Pleistocene stratified and scientifically dated faunal succession for the Indian subcontinent, stretching from MIS 7 (starting 240 ka) to the Holocene (MIS 1).

*Paleontological identification*

At Cathedral Cave, 144 of 5281 macrovertebrate bone fragments have been identified to genus or species level (SI Appendix Table S3), while in Charnel House Cave, 37 of 288 macrovertebrate bone fragments have been similarly identified to genus or species level (SI Appendix Table S4). The relatively low number of identified specimens is a result of taphonomic processes associated with external weathering and sedimentary transport of the remains into the caves.

Table 1 displays the presence or absence of genera and species from each Marine Isotope Stage represented by the Billasurgam sequence. Overall, the two Billasurgam caves present evidence for a diverse range of Middle–Late Pleistocene mammals, including small to large carnivores, primates, small to large bovids and cervids, rhinoceros and wild *Equus*. Crucially, every Pleistocene taxon identified survives in the Indian subcontinent today, with the exception of one primate based on a single specimen recovered in the 19$^{th}$ century excavations – here identified as *Theropithecus* cf. *gelada* (Fig. 3, SI Appendix Methods and Table S6a).

*Spatial comparison of faunal presence*

Genera and species in the Billasurgam sequence have been compared with the modern distributions of these taxa in the southern Indian state of Andhra Pradesh (20, 21) and India as a whole (21). This comparison indicates that the majority of taxa in the Billasurgam record are still present in modern Andhra Pradesh (20, 21). However, *Felis chaus* and *Ursus labiatus* are absent from the Billasurgam sequence following MIS 6, while *Herpestes griseus* and *Panthera pardus* are absent after MIS 5. Although *Herpestes griseus*, *Felis chaus, Ursus labiatus* and *Panthera pardus* are all still present in the wider Andhra Pradesh region today, they have a patchy distribution here, and in India as a whole. *Panthera pardus* is considered 'near threatened' (21), while the jungle habitat of *Felis chaus* has been greatly restricted in southern India. The broader continuity of these species in Andhra Pradesh is therefore tempered by restrictions to their previous distribution.

The fossil faunal record also includes mammalian taxa that are no longer present in the modern Billasurgam region. This has different implications for identifications depending on the taxonomic level being analyzed. Changes in the spatial distribution of a particular genus could be the result of either a spatial redistribution of species within that genus following

local extinctions or a new speciation event that has facilitated the persistence of a genus in new regions or environments. While a genus as a whole may demonstrate continuity, this level of identification cannot account for the extinction of past unidentified species within that genus. For example, although present in the Pleistocene layers of Billasurgam, no *Rhincoceros* sp. can be found anywhere in southern India today. Indeed, the Indian rhinoceros is currently restricted to heavily-forested and wetland habitats in northeast India and Nepal, with two thirds of the population confined to the Kaziranga National Park, Assam (21). This could either imply a restriction of range of the Pleistocene *Rhinoceros sp.* or a speciation event within that genus at a later stage that has led to the modern species. Similarly, *Equus hemionus khur* (Indian wild ass) is historically known from arid habitats of the subcontinent, including the Thar Desert and Baluchistan, but this endangered subspecies is currently restricted to the mesic Little Rann of Kutch (21). Again, its absence from modern Billasurgam could represent the restriction of range of a Pleistocene species or a more recent speciation event.

By contrast, changes in the spatial distribution of a particular species within India must be the result of range restriction in that species. Primate taxa are absent from the MIS 3 and 1/2 layers of the Billasurgam sequence (Table 1). However, comparisons of Lydekker's faunal identifications (14) with ours (SI Appendix Methods) suggest *Semnopithecus entellus* subsp. is present in layers corresponding to MIS 1 and 2. Fossil teeth of *S. entellus* from Billasurgam are closer in size to those of *S. entellus schistaceus*, today found in the Himalayan zone, than to those of the smaller subspecies *S. entellus entellus* found abundantly at Billasurgam today (SI Appendix Methods). This suggests that the range of the larger northern form may have extended significantly farther south during the later Pleistocene under cooler climatic conditions, or perhaps that local populations increased in size under those conditions following Bergmann's rule (22).

Of special interest is the presence of *Theropithecus* cf. *gelada* in the cave sequence during MIS 5 or earlier (Table 1, SI Appendix Methods). Extinct species of this genus are known from numerous sites in Africa between ~4 million years ago (Ma) and 200 ka, while the extant *T. gelada* is today restricted to the highlands of Ethiopia (23). How a *gelada*-sized species of *Theropithecus* might have reached southern India near the Middle–Late Pleistocene boundary is uncertain, although it suggests significant mobility of mammals during the later Pleistocene (24). *Theropithecus* specimens with larger inferred body size are known outside Africa in several areas: at ca. ~1.6 Ma in Israel, by 1.0 Ma in Europe (25) and at or after 1 Ma in northern India (26). Given the general trend in size increase over time in molar teeth of *Theropithecus oswaldi*, it is unlikely that any of these larger and older assemblages pertain to the ancestry of the Billasurgam species. However, it is not possible to determine whether the Billasurgam *Theropithecus* cf. *gelada* was part of an isolated group or belonged to a more widespread occurrence, nor when these relatives (or potentially conspecifics) of modern geladas first arrived in India.

**Discussion**

The fossil and contemporary data generally illustrate a continuation of mammalian genera and species in the Indian subcontinent from the late Middle Pleistocene to the present, a period encompassing two complete glacial–interglacial cycles, the deposition of ash from the Toba volcanic super-eruption, and the arrival of modern humans. The Billasurgam caves are close to abundant freshwater springs, recharged by rainfall from the humid Western Ghats, and as such they would have provided diverse wetland habitats capable of supporting a variety of mammals during periods of increased aridity. Continuity in faunal diversity at Billasurgam from MIS 7 to 5 suggests mammalian groups survived the penultimate glacial maximum in MIS 6. Although our data indicate that a number of genera and species were no longer present in the Billasurgam record after MIS 5, a nearby rockshelter excavation

indicates the survival of some of the smaller of these taxa, well into MIS 3 (27) and a number of these taxa are present in the wider Andhra Pradesh region today (20).

The continuity demonstrated by the Indian record is worth comparing with the well-studied faunal records from Southeast and Southwest Asia. The persistence of mammalian taxa in both the Indian and Sri Lankan Late Pleistocene records (28) indicates that the fauna of the Indian subcontinent were relatively resistant to climatic and human impacts associated with this period. Climatic instability during the last glacial cycle (29,30) may have resulted in local faunal turnover, such as the possible disappearance of large (>44 kg) carnivores in the Billasurgam record. Similarly, the disappearance of certain mammalian groups (especially those >44 kg) from the Billasurgam record after MIS 5, and particularly in MIS 3, could have been driven by increasing competition for fragmenting ecological resources from growing human populations, armed with microlithic technologies (31, 32). However, the relative stability of rainfall and topography across the Indian subcontinent as a whole meant that habitat survival in patches facilitated faunal recombination, migration, and general long-term persistence.

Resistance of mammalian fauna to environmental and human change has also been highlighted in records from mainland and island Southeast Asia (33). As in India, mixed, interconnected habitats facilitated long-term faunal persistence (34), including regional survival through the impact of the 74 ka Toba super-eruption (35). Although Southeast Asia witnessed the extinction or reduction in range of several genera (including *Stegodon*, *Hexaprotodon*, *Pongo*, *Crocuta*, *Hyaena*, *Tapirus* and *Rhinoceros*) during the late Middle Pleistocene, and increased faunal turnover and redistribution during the Late Pleistocene, this appears to have been generally limited to coastal areas vulnerable to eustatic changes in sea level and climate change linked to glacial cycles (36, 34). Here, rising sea levels fragmented

the linked, mosaic habitats permanently, resulting in isolated islands, such as Java, Sumatra and Flores, that were potentially more vulnerable to human, climatic, and ecological change.

The importance of stable mosaic habitats for faunal continuity is further demonstrated in the faunal records of Southwest Asia. The Levant (including Israel, Jordan, Lebanon and Syria) is often discussed in the context of environmental connectivity facilitating the migration of Pleistocene faunas (37). While cycles of aridity stimulated faunal turnover in the south and east of the Levant (38), the mosaic environment afforded by the foothills and forests of Israel's Mediterranean coastline facilitated stability of small and large mammalian taxa across the Middle and Late Pleistocene (39). As in the Indian record, the Israeli sequences indicate limited species turnover throughout the climatic cycles encompassed by MIS 7-2 (40, 41), with a resilience of Mediterranean fauna including *Gazella gazella*, and *Dama mesopotamica*. By contrast, the lack of mosaic environments in the deserts of the Arabian Peninsula meant that Arabian faunal communities were particularly vulnerable to extreme environmental fluctuations (42). Remains recovered from Middle Pleistocene lacustrine deposits demonstrate that species such as *Crocuta crocuta*, *Elaphas sp.,* and *Hexaprotodon* could survive in the deserts of the Arabian Peninsula under wetter conditions (43, 44). However the return of aridity and disappearance of freshwater sources led to the disappearance of these species from this region.

The Indian faunal record indicates long-term persistence of some mammals. On a genus level this is indicative of either new speciation events or species redistribution, while at a species level this demonstrates persistence of mammals within the subcontinent. The continued presence of 20 of 21 mammal taxa in the face of large-scale climatic changes, the Toba volcanic super-eruption, and human impacts throughout the Late Pleistocene mirrors the faunal record of general survivorship in Africa (2, 45). The continuation of faunal assemblages in Africa and India contrasts with the situation in northern Eurasia, Australia,

Madagascar, and the Americas, where many mammalian taxa became extinct prior to the Holocene (1–5), due perhaps in part to the influx of modern humans among other factors. Comparisons of the Indian faunal record with those from Southeast and Southwest Asia suggest that long-term faunal continuity is to be expected in the Asian tropics, unless disrupted by significant changes in rainfall or sea-level. In particular, interconnected mosaic habitats, facilitated by stability in topography and precipitation, have been essential to the long-term persistence of mammalian fauna across the Indian subcontinent. Recognition of the importance of ecological mosaics to mammalian survival is increasing in modern conservation studies in India and elsewhere in Asia (46). Moreover, increasing ecological circumscription in the face of demographic growth and environmental change in the most densely populated region of the world will present a significant challenge to mammals and those invested in their protection.

## Methods

### Optically Stimulated Luminescence (OSL) dating and stratigraphic correlations

OSL dating provides an estimate of the time elapsed since luminescent mineral grains were last exposed to sufficient heat or sunlight to empty the relevant electron traps. The method is based on the absorption of radiation energy by grains (quartz in this study) after the last heating or bleaching event, resulting in the trapping of electronic charge at defects in the crystal lattice. The population of trapped electrons increases with time after burial, in response to the supply of ionizing radiation from natural environmental sources (the 'dose rate'). The dose rate is mostly derived from the radioactive decay of $^{238}$U, $^{235}$U, $^{232}$Th (and their daughter products) and $^{40}$K in the deposits surrounding the dated mineral grains, together with smaller contributions from cosmic rays and from radioactive inclusions internal to the grains. Given the primary mode of sediment input to the Billasurgam cave complex (surface runoff and wind transport) and the lack of significant post-depositional reworking, the quartz grains

are likely to have been well bleached by sunlight at the time of burial and remained undisturbed thereafter.

For the OSL samples in this study, we measured the beta dose rates by low-level beta counting in the laboratory and the gamma dose rates in the field using *in situ* gamma-ray spectrometry. The cosmic-ray dose rates were determined using published equations, and a small contribution was assumed for the internal dose rate. Supporting data are provided in SI Appendix Methods. The radiation energy absorbed by the grains during the period of burial (the 'equivalent dose') was estimated in the laboratory by measuring the ultraviolet OSL emissions from individual grains of quartz (180–212 μm in diameter), to benefit from the advantages of single-grain OSL dating. A green laser was used to stimulate the most light-sensitive electron traps in each grain, and a dose-response curve was generated using the single-aliquot regenerative-dose procedure, from which the equivalent dose was estimated by interpolation. The OSL data were analysed using well-established and objective quality-assurance criteria and tests based on sound statistical principles. The burial age of each OSL sample was obtained by dividing the weighted mean equivalent dose (after rejecting outliers) by the dose rate. Details and data displays are given in SI Appendix Methods and the corresponding Figures, Tables and References.

Following numerical dating, the fossil record of faunal specimens was correlated with Marine Isotope Stages (MIS). This correlation was inferred on the basis of stratigraphic information (Fig. 2), the results of the OSL dating and the previous identification of Toba ash in the sequence of Charnel House Cave (19) (Fig. 2).

**Paleontological sampling and identification**

Faunal samples were excavated and collected by hand whenever possible. Samples were grouped on the basis of sediments excavated by a combination of natural layers and 10 cm spits within these layers. All sediments were dry sieved using 1 mm or 0.5 mm mesh in order to retrieve smaller

elements.

Taxonomic identifications were made with the aid of comparative modern osteological and late Quaternary fossil material housed in the Archaeozoology Laboratory at Deccan College. Faunal analysts Dr P.K. Thomas (former Director, Archaeozoology Laboratory), and Dr P. Joglekar helped with the analysis of several difficult specimens. SI Appendix Tables S1 and S2 demonstrate the skeletal elements used to identify different genera and species. In all cases, elements were only identified to genus or species level when an excavated element was considered indistinguishable from the modern and fossil reference taxa. Carnivora from the two sites were identified on the basis of dental, phalangeal, humeral and femoral measurements. Primates were primarily identified using dental measurements, though some cranial comparisons were also possible. Bovids, cervids and other Artiodactyla were similarly taxonomically categorized on the basis of dental fragments, astragali, distal phalanges, and long bone measurements. The identification of *Equus* sp. from both sites relied upon a comparison of dental remains with the modern collections, while *Rhinoceros* sp. identification was based on dental remains at Cathedral Cave and rib fragments at Charnal House Cave. Further detail of each taxonomic identification is provided in SI Appendix Tables S1 and S2.

Given the highly fragmentary nature of the skeletal material, taxonomic abundances are quantified according to specimen counts (number of identifiable faunal specimens, NISP). Following specimen identification, the presence or absence of each identified genus/species was recorded relative to the correlated MIS. This provides the best representation of faunal diversity at Billasurgam through time. For further detail see SI Appendix SI Methods.

**Spatial comparison of faunal presence**

Following correlation of the presence of fossil taxa with the MIS chronology, the fossil faunal record was compared with modern faunal diversity studies from the State of Andhra Pradesh of which Billasurgam is a part (20). The fossil faunal record was also compared to records held by the International Union for Conservation of Nature (21) of modern faunal distributions across modern

India. This was done in order to track changes in the spatial distributions of fauna in India and surrounding regions through time.

## Acknowledgments

This project was funded by grants from the British Academy, the Leverhulme Trust and the European Research Council (grant no. 295719) (to M.D.P.) and the Australian Research Council (to R.G.R.). We thank the Archaeological Survey of India for permission to conduct the fieldwork and the international team for their contributions to the excavations. We thank Miriam Belmaker, John de Vos, and Chris Stimpson for suggestions regarding faunal continuity in the Levant, Southeast Asia, and the Arabian Peninsula respectively.

## Additional Information

**Author contributions** M.D.P. and P.R. conceived the project; P.M. collected all mammalian specimens and identified mammalian specimens including some primates; E.D., R.L.C., J.G.F., S.R.F., C.C.G., G.F.G. and T.H. identified primate specimens including the *Theropithecus* specimen from 19th century excavations and provided comparative metrical data; R.G.R. and Z.J. scientifically dated the sequence; P.R. and P.D. collected and analyzed the stratigraphic data; M.D.P., P.R., E.D., R.G.R. and the other authors contributed to the preparation and writing of the manuscript.

The authors declare no **conflict of interest**.

**Supporting Information Appendix** accompanies this main text and includes

SI Appendix Methods:

Fossil identification methodology (including primate identification methodology)

Correlation of stratigraphic units with 19$^{th}$ century excavations

Optically stimulated luminescence (OSL) dating

SI Appendix Figures S1, S2, S3

SI Appendix Tables S1, S2, S3, S4, S5, S6, S7, S8, S9, S10, S11

SI Appendix reference list

**References**


1. Rule S, et al. (2012) The aftermath of megafaunal extinction: ecosystem transformation in Pleistocene Australia. *Science* 335: 1483-1486.

2. Koch PL, Barnosky AD (2006) Late Quaternary extinctions: state of the debate. *Annu Rev Ecol Evol S* 37: 215-250.

3. Prideaux GJ, et al. (2010) Timing and dynamics of Late Pleistocene mammal extinctions in southwestern Australia. *P Nat Acad Sci USA* 107: 22157-22162.

4. Lorenzen ED, et al. (2011) Species-specific responses of Late Quaternary megafauna to climate and humans. *Nature* 479: 359-364.

5. Prescott GW, Williams DR, Balmford A, Green RE, Manica A (2012) Quantitative global analysis of the role of climate and people in explaining late Quaternary megafaunal extinctions. *P Nat Acad Sci USA* 109: 4527-4531.

6. Brace S, et al. (2012) Serial population extinctions in a small mammal indicate Late Pleistocene ecosystem instability. *P Nat Acad Sci USA* 109: 20532-20536.

7. Boivin N, Fuller DQ, Dennell R, Allaby R, Petraglia MD (2013) Human dispersal across diverse environments of Asia during the Upper Pleistocene. *Quatern Int* 300**:** 32-47.

8. Badam GL, (1979) *Pleistocene Fauna of India* (Deccan College Postgraduate and Research Institute, Pune, India).

9. Clift PD, Plumb RA (2008) *The Asian Monsoon: Causes, History and Effects* (Cambridge University Press).

10. Petraglia MD, Haslam M, Fuller DQ, Boivin N, Clarkson C (2010) Out of Africa: new hypotheses and evidence for the dispersal of *Homo sapiens* along the Indian Ocean rim. *Ann Hum Biol* 37: 288-311.

11. Mellars P, Goric KC, Carr M, Soares PA, Richards MB (2013) Genetic and archaeological perspectives on the initial modern human colonization of southern Asia. *P Nat Acad Sci USA.* 110: 10699-10704.

12. Blinkhorn J, Parker AG, Ditchfield P, Haslam M, Petraglia M (2012) Uncovering a landscape buried by the super-eruption of Toba, 74,000 years ago: a multi-proxy environmental reconstruction of landscape heterogeneity in the Jurreru Valley, south India. *Quatern Int* 258: 135-147.

13. Foote RB (1885) Notes on the results of Mr H.B. Foote's further excavations in the Billa Surgam caves. *Records of the Geological Survey of India* 18: 227-235.

14. Lydekker R (1886) The fauna of the Kurnool Caves. *Palaeontologica Indica Series X* 4: 23-58.

15. Murty MLK (1974) A Late Pleistocene cave site in southern India. *P Am Philos Soc* 118: 196-230.

16. Reddy KT (1977) Billasurgam: An Upper Palaeolithic Cave Site in South India. *Asian Perspect* 20: 206-277.

17. Petraglia MD, et al. (2009) Human occupation, adaptation and behavioral change in the Pleistocene and Holocene of South India: recent investigations in the Kurnool District, Andhra Pradesh. *Eurasian Prehistory* 6: 119-166.

18. Haslam M, et al. (2010) In Foote's steps: the history, significance and recent archaeological investigation of the Billa Surgam caves in southern India. *S Asian Stud* 26: 1-19.

19. Lane C, et al. (2011) Cryptotephra from the 74 ka BP Toba super-eruption in the Billa Surgam caves, southern India. *Quaternary Sci Rev* 30: 1819-1824.

20. Srinivasulu C, Nagulu V (2002) Mammalian and Avian Diversity of the Nallamala Hills, Andhra Pradesh. *Zoos' Print Journal* 17: 675-684.

21. International Union for Conservation of Nature, http://www.iucnredlist.org

22. Meiri S, Dayan T (2003) On the validity of Bergmann's rule. *J Biogeogr* 30**:** 331-351.

23. Jablonski NG, Frost SR (2010) Cercopithecoidea. *Cenozoic Mammals of Africa* eds Werdelin L, Sanders WJ (University of California Press, Berkeley), pp. 393–428.

24. Hughes JK, Elton S, O'Regan HJ (2008) *Theropithecus* and 'Out of Africa' dispersals in the Plio-Pleistocene. *J Hum Evol* 54: 43-77.

25. Rook L, Martínez-Navarro B (2013) The large sized cercopithecoid from Pirro Nord and the importance of *Theropithecus* in the Early Pleistocene of Europe: faunal marker for hominins dispersal outside Africa. *Palaeontographica Abteilung A* 298**:** 107-112.

26. Delson E (1993). *Theropithecus* fossils from Africa and India and the taxonomy of the genus. *Theropithecus: Rise and Fall of a Primate Genus* ed Jablonski NG (Cambridge University Press, Cambridge), pp. 157–189.

27. Clarkson C, et al. (2009) The oldest and longest enduring microlithic sequence in India: 35 000 years of modern human occupation and change at the Jwalapuram Locality 9 rockshelter. *Antiquity* 83: 326-348.

28. Perera N, et al. (2011) People of the ancient rainforest: Late Pleistocene foragers at the Batadomba-lena rockshelter, Sri Lanka. *J Hum Evol* 61: 254-269.

29. Prabhu CN, et al. (2004) A 200-ka pollen and oxygen-isotopic record from two

sediment cores from the eastern Arabian Sea. *Palaeogeogr Palaeocl* 214: 309-321.

30. Caley T, et al. (2011) New Arabian Sea records help decipher orbital timing of Indo-Asian monsoon. *Earth Planet Sc Lett* 308: 433-444.

31. Atkinson QD, Gray RD, Drummond AJ (2008) mtDNA variation predicts population size in humans and reveals a major Southern Asian chapter in human prehistory. *Mol Biol Evol* 25**:** 468-474.

32. Petraglia M, et al. (2009) Population increase and environmental deterioration correspond with microlithic innovations in South Asia ca. 35,000 years ago. *P Nat Acad Sci USA.* 106: 12261-12266.

33. Louys J (2012) Mammal community structure of Sundanese fossil assemblages from the Late Pleistocene, and a discussion on the ecological effects of the Toba eruption. *Quatern Int* 258: 80-87.

34. Louys J, Meijaard E (2010) Palaeoecology of Southeast Asian megafauna-bearing sites from the Pleistocene and a review of environmental changes in the region. *J Biogeogr* 37: 1432-1449.

35. Louys J (2007) Limited effect of the Quaternary's largest super-eruption (Toba) on land mammals from Southeast Asia. *Quaternary Sci Rev* 26: 3108-3117.

36. Long VT, de Vos, J, Ciochon RL (1996) The fossil mammal fauna of the Lang Trang Caves, Vietnam compared with Southeast Asian fossil and recent mammal faunas: the geographica; implications. *Bull Indo Pac Pre Hi* 14. 1: 101-109.

37. Tchernov E (1988) The biogeographical history of the southern Levant. *The Zoogeography of Israel* eds Yom-Tov Y, Tchernov E (Dr. Junk Publishers, Dordrecht), pp. 159-250.

38. Belmaker M (2009) Hominin adaptability and patterns of faunal turnover in the Lower-Middle Pleistocene transition in the Levant. *A Sourcebook of Paleolithic Transitions: Methods, Theories and Interpretations* eds Camps M, Chauhan PR (Springer), pp. 211-227.

39. Belmaker M, Hovers E (2011) Ecological change and the extinction of the Levantine Neanderthals: implications from a diachronic study of micromammals from Amud Cave, Israel. *Quaternary Sci Rev* 30: 3196-3209.

40. Mercier N, et al (2007) Hayonim Cave: a TL-based chronology for this Levantine Mousterian sequence. *J Archaeol Sci* 34:1064-1077.

41. Marder O, et al (2011) Mammal remains at Rantis Cave, Israel, and Middle-Late Pleistocene human subsistence and ecology in the Southern Levant. *J Quaternary Sci* 26: 769-780.

42. Groucutt HS, Petraglia MD (2012) The Prehistory of the Arabian Peninsula: Deserts, Dispersals, and Demography. *Evol Anthropol* 21:113–125

43. Thomas H, et al (1998) First Pleistocene faunas from the Arabian Peninsula: An Nafud desert, Saudi Arabia. *CR Acad Sci II A* 326: 145-152.

44. Rosenberg TM, et al (2013) Middle and Late Pleistocene humid periods recorded in palaeolake deposits of the Nafud desert, Saudi Arabia. *Quaternary Sci Rev* 70: 109-123.

45. Faith JT (2014) Late Pleistocene and Holocene mammal extinctions on continental Africa. *Earth-Sci Rev* 128: 105-121.

46. Cranbrook E, Piper PJ (2013) Paleontology to policy: the Quaternary history of Southeast Asian tapirs (Tapiridae) in relation to large mammal species turnover, with

a proposal for conservation of Malayan tapir by reintroduction to Borneo. *Integrative Zoology* 8: 95-120.

**Figure Legends**

**Fig. 1.** Map of the Billasurgam cave complex, showing the positions of the excavations at Charnel House Cave and Cathedral Cave at its northern and southern ends, respectively.

**Fig. 2.** Composite sedimentary log of the sequences in the Charnel House and Cathedral chambers of the Billasurgam cave complex. The deposits are composed of silt-dominated cave earths, punctuated by bands of angular blocky limestone conglomerate (from roof/wall collapse) and more rounded, mixed pebble conglomerate bands (input by land surface runoff via sink hole depositional processes). Inferred correlation of the layers by Marine Isotope Stage (MIS) is based on stratigraphic inferences, OSL dating of the sediments, and the identification of Youngest Toba Tuff (YTT) ash shards. Wavy lines indicate disconformities with missing sediment, whereas dashed lines are estimated boundaries in semi-continuous sections. Several of the OSL ages fall on or near the ages assigned to MIS boundaries, so the plotted boundary positions and MIS designations are approximate.

**Fig. 3.** *Theropithecus* cf. *gelada* lower second (?) molar from Bed M of Charnel House Cave, correlated here to at least 74 ka, MIS 5 or older; left to right, occlusal, buccal and lingual views (photos by R.L.C).

**Table 1.** Faunal succession at the Billasurgam Caves, arranged by Marine Isotope Stage (MIS).

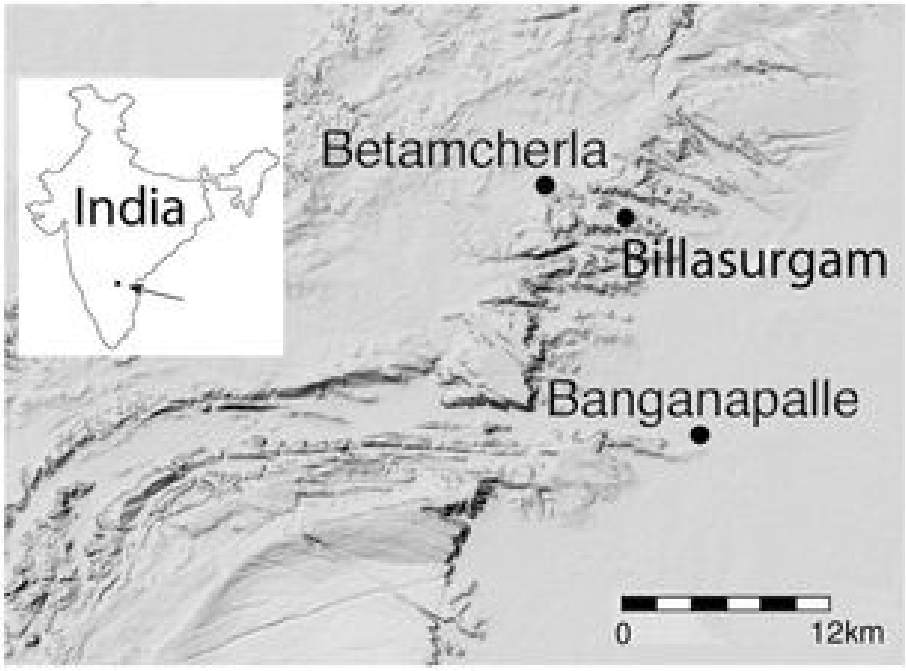


Charnel House

N

*stream-bed*

Cathedral

cave wall

Chapter House

0 50m

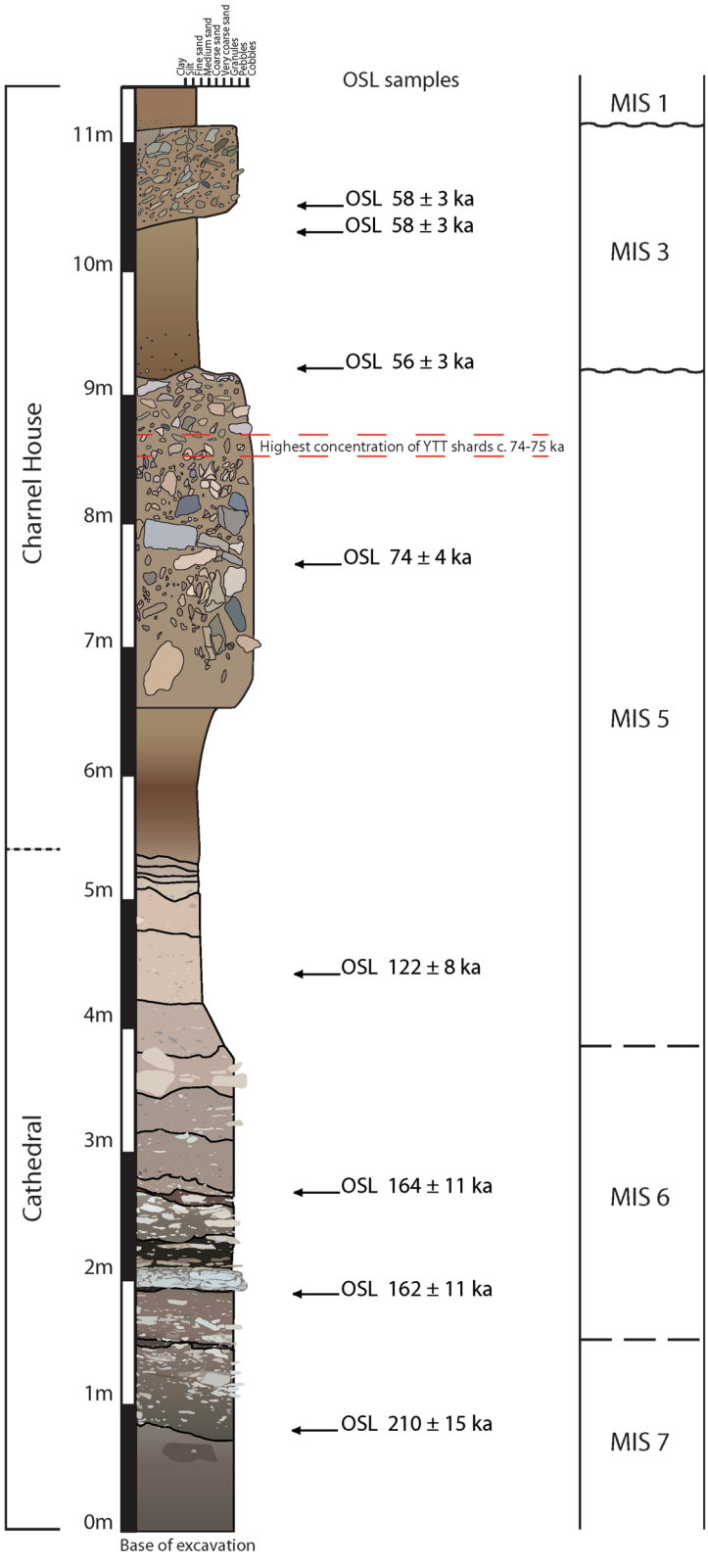
Clay
Silt
Fine sand
Medium sand
Coarse sand
Very coarse sand
Granules
Pebbles
Cobbles
OSL samples
MIS 1
MIS 3
MIS 5
MIS 6
MIS 7
Charnel House
Cathedral
11m
10m
9m
8m
7m
6m
5m
4m
3m
2m
1m
0m
OSL 58 ± 3 ka
OSL 58 ± 3 ka
OSL 56 ± 3 ka
Highest concentration of YTT shards c. 74-75 ka
OSL 74 ± 4 ka
OSL 122 ± 8 ka
OSL 164 ± 11 ka
OSL 162 ± 11 ka
OSL 210 ± 15 ka
Base of excavation


F2 01A
1 cm

**Table 1. Faunal succession at the Billasurgam Caves, arranged by Marine Isotope Stage (MIS).**

| | Modern India[1] | Modern Andhra Pradesh[2] | MIS 1 | MIS 3 | MIS 5 | MIS 6 | MIS 7 |
|---|---|---|---|---|---|---|---|
| **Carnivora** | | | | | | | |
| *Ursus* sp. | + | + | | | | + | |
| *Felis chaus* | + | + | | | | + | |
| *Panthera pardus* | + | + | | | + | | |
| *Herpestes griseus* | + | + | | | + | + | |
| *Canis* sp. | + | + | | | + | + | |
| *Vulpes* sp. | + | + | | | + | + | |
| **Primates** | | | | | | | |
| *Theropithecus* cf. *gelada* | | | | | + | | |
| *Semnopithecus entellus* subsp. | + | + | | | +[3] | | |
| **Artiodactyla** | | | | | | | |
| *Bos* sp. | + | + | | | + | + | |
| *Boselaphus* sp. | + | + | | | + | + | + |
| *Antilope cervicapra* | + | + | | | + | + | |
| *Gazella* sp. | + | + | | | + | + | + |
| *Tetracerus quadricornis* | + | + | | + | + | | |
| *Axis axis* | + | + | + | | + | + | |
| *Muntjacus* sp. | + | + | | | | + | |
| *Sus* sp. | + | + | | | + | + | |
| **Other** | | | | | | | |
| *Equus* sp. | + | | | + | + | + | + |
| *Rhinoceros* sp. | + | | | + | + | + | |
| *Lepus* sp. | + | + | + | + | + | + | |
| *Hystrix crassidens* | + | + | | + | + | + | |
| *Erinaceus* sp. | + | + | | | + | | |

+ Specimens identified in this study, including our re-examination of *Theropithecus* cf. *gelada* specimen from 19th century excavations.

[1] As known in the records of the International Union for Conservation of Nature (21)

[2] As known from modern faunal studies of Andhra Pradesh (20)

[3] Provides a *terminus ante quem*. *Theropithecus* specimen comes from Foote's excavations, which removed layers that are now minimally dated to MIS 5. The actual date remains unknown due to the removal of these layers (SI Methods).

# Supporting Information Appendix for: Continuity of Mammalian Fauna Over the Last 200,000 Years in the Indian Subcontinent

Patrick Roberts[1], Eric Delson[2, 3], Preston Miracle[4], Peter Ditchfield[1], Richard G. Roberts[5], Zenobia Jacobs[5], James Blinkhorn[6], Russell L. Ciochon[7], John Fleagle[8], Stephen R. Frost[9], Christopher C. Gilbert[10], Gregg F. Gunnell[11], Terry Harrison[12], Ravi Korisettar[13], Michael D. Petraglia[1,14]

[1] School of Archaeology, Research Laboratory for Archaeology and the History of Art, University of Oxford, Dyson Perrins Building, South Parks Road, Oxford OX1 3QY, UK.

[2] Department of Vertebrate Paleontology, American Museum of Natural History, New York, NY 10024, USA.

[3] Department of Anthropology, Lehman College/City University of New York, Bedford Park Boulevard West, Bronx, NY 10468 USA; and The Graduate Center, City University of New York and New York Consortium in Evolutionary Primatology, New York, NY 10016, USA.

[4] Division of Archaeology, University of Cambridge, Downing Street, Cambridge CB2 3DZ, UK.

[5] Centre for Archaeological Science, School of Earth & Environmental Sciences, University of Wollongong, Wollongong, New South Wales 2522, Australia.

[6] PACEA, Université Bordeaux 1, Bâtiment B 18, Avenue des Facultés, 33405 Talence Cedex, France.

[7] Department of Anthropology and Museum of Natural History, University of Iowa, Iowa City, IA 52242 USA

[8] Anatomical Sciences, School of Medicine, Stony Brook University, Stony Brook, NY 11794-8081 USA.

[9] Department of Anthropology, University of Oregon, Eugene, OR 97132-1218 USA.

[10] Department of Anthropology, Hunter College/City University of New York, 695 Park Avenue, New York, NY 10065 USA; and The Graduate Center, City University of New York and New York Consortium in Evolutionary Primatology, New York, NY 10016, USA.

[11] Division of Fossil Primates; Duke Lemur Center; 1013 Broad Street; Durham, NC 27705 USA; and The Graduate Center, City University of New York and New York Consortium in Evolutionary Primatology, New York, NY 10016, USA.

[12] Center for the Study of Human Origins, Department of Anthropology, New York University, 25 Waverly Place, New York, NY 10003, USA and New York Consortium in Evolutionary Primatology, New York, NY 10016, USA.

[13] Department of History and Archaeology, Karnatak University, Dharwad 580-003, India

[14] Human Origins Program, Smithsonian Institution, Washington, DC, 20560 USA.

correspondence to: Michael D. Petraglia
email: michael.petraglia@rlaha.ox.ac.uk
School of Archaeology, Research Laboratory for Archaeology and the History of Art, University of Oxford, Dyson Perrins Building, South Parks Road, Oxford OX1 3QY, UK
Telephone: +441865 275373

## This PDF file includes:

## SI Methods

**Fossil identification methodology.** Recovered faunal samples were sorted in the field into "identifiable" and "unidentifiable" components. Those classified as "identifiable" remains include: all specimens greater than 5 cm in length, all teeth, all fragments with an articular end (or significant portion thereof), and all long-bone shafts with a nutrient foramen, significant anatomical landmark, and/or with the entire circumference of the shaft preserved. Faunal samples classified as "unidentifiable" were generally small splinters of long bones and bits of spongy bone not identifiable to element. Rib shafts smaller than 5 cm and lacking the head and/or tubercle were also treated as "unidentifiable". Similarly, cranial fragments lacking readily identifiable landmarks that were smaller than 5 cm were categorized as "unidentifiable".

As stated in the main text, taxonomic identifications were then made on the basis of comparison with modern osteological and late Quaternary fossil material housed in the Archaeozoology Laboratory at Deccan College. Faunal analysts Dr P.K. Thomas (former Director, Archaeozoology Laboratory), and Dr P. Joglekar helped with the analysis of several difficult specimens. Tables S1 and S2 provide detail regarding the different skeletal elements used to identify genera and species. Elements could only be identified to genus or species level when an excavated element was considered indistinguishable from either the modern and fossil reference taxa.

**Primate identification methodology** *(GSI - Geological Survey of India, Kolkata)*. Lydekker (14) described jaws of *Semnopithecus entellus* from Beds A and M of Charnel House Cave, as well as more fragmentary material from Cathedral Cave. He noted that these were larger than *S. [entellus] priam* and similar in size to the large *S. [entellus] schistaceus*, but he thought it highly unlikely that the Billasurgam fossils might belong to the latter (sub)species, presumably because they only occurred in the Himalayan zone far to the north. In fact, the teeth agree closely in size with those of *S. entellus schistaceus* and *S. entellus ajax* (Table S6b).

In addition, a concentration of primate bones was recovered in 2009 in Charnel House Cave from layers dated to MIS 5. Taxonomic identification was based on comparisons made (by PM) using high-resolution photos of baboon skeletal elements (*Papio* [*hamadryas*] *cynocephalus* from

"www.eskeletons.org", based at the University of Texas, Austin), and macaque skeletons (*Macaca mulatta*) from Deccan College drawn from males and females of various sizes. Comparisons were also made to a single skeleton of a juvenile langur (*Semnopithecus entellus*), also from Deccan College. In all cases fossil elements were identified as *S. entellus*, although confidence varies, and it is possible that some may have come from *Macaca* individuals. Several well-preserved bones were larger than their homologues in a female *S. e. entellus*, but it was not possible to determine the sex of the fossil bones, so their subspecific identity remains uncertain.

The most interesting primate tooth from the Billasurgam caves is an isolated lower molar, probably a second, GSI No. F. 202, from Bed M of Charnel House Cave, which Lydekker attributed to *Cynocephalus* sp., the African baboon (i.e., *Papio*). Lydekker (14) (p. 29) wrote: "In its very large size, tall crown, and form of the cusps, this specimen differs widely from the teeth of *Semnopithecus* and *Macacus*, and agrees so exactly with those of *Cynocephalus* that there can be no doubt as to its belonging to that genus." For the century following this publication, authors referring to this specimen generally thought it came from a large macaque, but most ignored it as the deposits were thought to be latest Pleistocene or Holocene in age. In the last decade, several of the authors (TH, later confirmed by RLC and GFG) located and reassessed the identity of this tooth, determining that it belonged to the genus *Theropithecus*, due to its diagnostic occlusal morphology that is not well portrayed in Lydekker's figure. It presents almost no wear, clearly showing the high occlusal relief, columnar cusps and deep mesial clefts that typify the molars of *Theropithecus* (47) (Fig. 3). Analysis of the size of this tooth (Table S6a) reveals that it is a close match for the $M_2$ of extant *Theropithecus gelada*, otherwise known only from the highlands of Ethiopia. Study of mtDNA from several living populations (48) suggested that they diverged ca 1 Ma, implying that the species was present in Ethiopia by this time, although there is no fossil record in Africa.

In addition, the genus is known by three extinct species. *Theropithecus brumpti* is entirely restricted to the Turkana Basin of Northern Kenya and Southern Ethiopia and the nearby Baringo Basin of Kenya, while *T. baringensis* comes from the Baringo Basin (and perhaps the Turkana Basin)(23). The third species, *T. oswaldi*, is widely viewed as the sister taxon to *T. gelada* and comes from numerous

sites in eastern, southern and northern Africa between ca. 4 Ma and 200 ka. *T. oswaldi* shows significant size increase through time from the earliest populations (*T. oswaldi darti*) close in size to the extant species through *T. oswaldi oswaldi* to "giant" *T. oswaldi leakeyi* with molar teeth nearly twice the length and mass up to 5 times as great as in extant *T. gelada* (25, 49).

Outside Africa, the most definite occurrence in the circum-Mediterranean region is at Cueva Victoria (Spain, ca. 1 Ma), where one published tooth (24) is comparable in size to those of large *T. oswaldi*. Rare postcranial elements have been more controversially identified as *Theropithecus* from 'Ubeidiya (Israel, ca. 1.6 Ma), and especially Pirro Nord (Italy, ca. 1.3 Ma) (24). One fragment of a maxilla with worn upper second and third molars was described from Mirzapur, northern India, as *Theropithecus delsoni*, later reassigned to *Theropithecus oswaldi delsoni* (25). Measurements of these teeth (Table S6a) show them to be larger than the mean (and close to the known maxima) for *T. oswaldi oswaldi*, far larger than expected for uppers of *T.* cf. *gelada* from Billasurgam.

**Correlation of stratigraphic units with 19th century excavations.** Fossils identified in the 19th century excavations in the Billasurgam caves were correlated with the modern stratigraphic succession and its chronological sequence. In some cases Lydekker (14) identified taxa not present in our faunal analysis of the 2003-2008 excavations at the caves (Table S5). The correlation of Foote's stratigraphic excavation notes and the 2003-2008 excavation notes and chronology are shown in Tables S7 and S8. This is based on Foote's 19th century report (13) and stratigraphic records from the 2003-2009 excavations at the complex (Fig. 2).

Charnel House Cave:

We correlate Foote's Beds A1, A, B and C with MIS 1/MIS 2 on the basis of pottery found in Foote's excavations and the 2003-2009 excavations. Foote describes his Beds D and E as being within a "rubble bed". We correlate these layers with the upper rubble section shown in Fig. 2 that is dated at its base to 58 ± 3 ka and therefore MIS 3. Foote notes that his Beds H, I and J consist of red to red-brown cave earth. We correlate these layers with the underlying red earth layers in Fig. 2 that are bracketed by the dates of 58 ± 3 ka and 56 ± 3 ka respectively. This would place these Beds within MIS 3. Foote describes Beds K and L as "Red sandy cave earth with blocks of limestone". We therefore correlate these layers with the second rubble section from Charnel House Cave shown in Fig. 2. The top of this section is dated to *c*. 74 ka by Young Toba tephra shards, and also by an OSL date of 74 ± 4 ka in the middle of the section. This would place Foote's Beds K and L within MIS 5. Foote describes Beds M and N, within which the identified *Theropithecus* specimen was found (SI Methods), as consisting of a "stiff marly clay". These layers were unavailable in the 2003-2009 excavations due to complete removal by Foote in the 19th century. However, given the stratigraphic information we can broadly state that these layers are either MIS 5 or earlier.

Cathedral Cave:

Foote's Beds C, Ca, Cb and CC were completely cleared during the 19th century excavations. His notes remain our only surviving record of these deposits. However, given the large number of specimens identified by Lydekker (14) from these levels, we have included these Beds in Table S4. We have used the underlying MIS 5 levels as a *terminus ante quem*. No further precision is possible. Foote notes that the excavation of Bed Cd exposed the mouth of the passage leading to the Fairy

Chamber (Fig. 1). Foote removed half of this layer, while half remained. We correlate this layer with the commencement of excavations at Cathedral Cave in 2003-2008. This layer is dated by an OSL date of 122 ± 8 ka towards the top of this area of excavation. This would place Foote's Bed Cd in MIS 5. Foote describes Beds Ce and Cf as "stiff dark marl". A similar material is found below the stiff red clay that represented the remains of bed Cd prior to excavation and is dated by an OSL date of 164 ± 11 ka at its base. Foote recorded Bed Ch as a "Dark loamy marl" which was not identified in the 2003-2009 excavations and therefore no correlation has been attempted. Foote describes Beds Ci, Cj, Ck and Cl as "grey marl". These layers appear to correspond to the more sterile material found at the base of the 2003-2008 excavations. However, within these layers there are OSL dates from 162 ± 11 ka at the top of this material to 210 ± 15 ka in the middle of the section. Without any further stratigraphic information it is impossible to correlate these Beds more precisely than to MIS 6/7.

**Optically stimulated luminescence (OSL) dating**. OSL dating provides an estimate of the time since grains of quartz or feldspar were last exposed to sunlight (50–52). In this study, we estimated the burial time of individual sand-sized grains of quartz to benefit from the advantages of single-grain OSL dating (53, 54). The burial age is estimated by dividing the equivalent dose ($D_e$, a measure of the radiation energy absorbed by a grain during the period of burial) by the environmental dose rate (the rate of supply of ionising radiation to the grain over the same period). The $D_e$ is determined from laboratory measurements of the OSL signals, and the dose rate is estimated from laboratory and field measurements of the environmental radioactivity (and the small contribution from cosmic rays).

Four sediment samples for OSL dating were collected from the Charnel House Cave deposits and a further four from Cathedral Cave. Their stratigraphic positions are shown in Fig. 2, and a photograph of the sampled section in Charnel House Cave is shown in Fig. 1 of Lane *et al*. (19). Samples were collected by hammering metal tubes into the cleaned section faces, after which the tubes were removed and sealed in black plastic bags for safe transport to the University of Wollongong. Additional sediment samples were collected for laboratory measurements of radioactivity and the tube holes were used for field measurements of the dose rate from gamma rays, which can penetrate up to 30 cm through most sedimentary deposits. The tubes were opened under dim red light in the laboratory and quartz grains were extracted from the interior of each tube using standard procedures (51, 55). First, carbonates were dissolved in 10% hydrochloric acid and then organic matter was oxidised in 30% hydrogen peroxide solution. The residue was dried and then sieved to isolate grains of 180–212 μm in diameter, and feldspar and heavy minerals were removed by density separation using sodium polytungstate solutions of 2.62 and 2.70 specific gravities, respectively. The separated quartz grains were etched in 48% hydrofluoric acid for 40 min (to remove their alpha-irradiated rinds and destroy any remaining feldspar grains) and then rinsed in hydrochloric acid, dried and sieved again; grains retained on the 180 μm diameter mesh were used for dating.

Single-grain OSL measurements were made using the same instruments and single-aliquot regenerative-dose (SAR) procedures as those employed previously to date quartz grains from sites in the Jurreru River valley, located 14 km south-southwest of the Billasurgam cave complex (56, 57). The SAR procedure (58, 59) involves measuring the OSL signals from the natural (burial) dose and

from a series of regenerative doses (given in the laboratory by means of a calibrated beta source), each of which were preheated at 260°C for 10 s prior to optical stimulation by a green (532 nm) laser beam for 2 s at 125°C. A small test dose (preheated at 160°C for 10 s) was given after each natural and regenerative dose, and the resulting OSL signals were used to correct for any sensitivity changes. A duplicate regenerative dose was included in the procedure, to check on the adequacy of this sensitivity correction, and a 'zero dose' measurement was made to monitor the extent of any 'recuperation' induced by the 260°C preheat.

The ultraviolet OSL emissions were detected by an Electron Tubes Ltd 9235QA photomultiplier tube fitted with Hoya U-340 filters. The $D_e$ values were estimated from the first 0.2 s of OSL decay, with the mean count recorded over the last 0.3 s being subtracted as background. Dose-response curves were fitted to the sensitivity-corrected regenerative-dose points using a single saturating exponential or saturating exponential plus linear function. The $D_e$ was obtained by projecting the sensitivity-corrected natural signal on to this curve (59), after adding (in quadrature) an instrumental reproducibility uncertainty of 2% to the photon counting statistics for each OSL measurement (60), and the standard error of this $D_e$ estimate was determined by Monte Carlo simulation.

Grains with OSL properties unsuitable for the SAR procedure were rejected using well-established and objective quality-assurance criteria, which are listed in the footnotes to Table S9 and are described in detail elsewhere (53, 61–67). The experimental conditions and methods of data analysis were chosen on the basis of dose recovery tests (68) performed on quartz grains from the Jurreru River valley (57). Two samples were bleached at room temperature and then given a known beta dose before any OSL measurements. Ratios of measured/given dose of 0.996 ± 0.034 and 0.985 ± 0.015 were obtained using the same experimental and analytical procedures as employed in this study, which indicates that they can accurately recover the correct dose under controlled conditions.

The environmental dose rate is due mainly to beta and gamma radiation from the nuclear decay of $^{238}U$, $^{235}U$, $^{232}Th$ (and their daughter products) and $^{40}K$ in the deposits surrounding the dated grains. There are additional, albeit small, contributions to the dose rate from alpha emitters inside the quartz

grains and from cosmic radiation. Beta dose rates were measured directly by low-level beta counting of dried, homogenised and powdered sediment samples in the laboratory, using a GM-25-5 multicounter system (69). To check the equilibrium status of the $^{238}U$ and $^{232}Th$ decay chains, high-resolution gamma-ray spectrometry (HRGS) measurements were made on the powdered splits of two samples (CHAR-1 and CHAR-2), using the same intrinsic germanium detectors and international calibration standards as described by Olley *et al*. (70, 71). Allowance was made for the effect of grain size and hydrofluoric acid etching on the beta dose rate, and two systematic errors (each of 3%) were included in the uncertainty. Gamma dose rates were measured at each sample location by *in situ* gamma spectrometry; a Na(Tl) detector was inserted into the holes left after removing the metal tubes. Details of equipment and analytical methods follow those described by Jacobs *et al*. (64).

The total dose rate for each sample includes an assumed effective internal dose rate of 0.032 Gy/ka and a cosmic-ray dose rate estimated following Prescott and Hutton (72). The latter was adjusted for the geomagnetic latitude and altitude of each cave, as well as the thickness and density of sediment and limestone shielding each sample (averaged over the full period of burial and accounting for the prior removal of the upper deposits by Foote). The beta, gamma and cosmic-ray dose rates were corrected for the estimated long-term water content of each sample, using values up to a few percent higher than the measured (field) values to allow for sample collection during the dry season and desiccation of the section faces after excavation (Table S10). Uncertainties were assigned to encompass (at $2\sigma$) the measured values and plausible long-term variations integrated over the entire period of sample burial. Lower water contents (one-half of the values shown in parentheses in Table S10) were used to calculate the gamma dose rates for samples CHAR-3, CHAR-4 and CATH-3, to make allowance for the limestone cobbles and boulders in these rubble layers, and no water correction was applied to the cosmic rays passing through the limestone roof of either cave. The calculated ages increase (or decrease) by ~1% for each 1% increase (or decrease) in water content, so they are not especially sensitive to the values used.

The radionuclide activities determined from HRGS measurements on samples CHAR-1 and CHAR-2 are shown in Table S11, together with the beta dose rates calculated from them. The latter are

statistically consistent with the beta dose rates estimated by GM-25-5 beta counting, so the weighted mean values (listed in Table S9) were used to calculate the total dose rates for these two samples. The HRGS analyses show that the $^{232}$Th decay chain (represented by $^{228}$Ra and $^{228}$Th in Table S10) is presently in a state of secular equilibrium, as is typically the case for terrestrial sediments. The $^{238}$U decay chain (represented by $^{238}$U, $^{226}$Ra and $^{210}$Pb) has only minor deficits of $^{238}$U and $^{210}$Pb relative to $^{226}$Ra, which we attribute to the leaching of uranium by groundwater and the loss of radon gas to atmosphere, both of which are commonplace in limestone cave deposits (73−75). We have assumed that these conditions prevailed throughout the period of sample burial, but numerical modelling has shown that even the most common time-dependent disequilibria in the $^{238}$U series are unlikely to give rise to errors in the total dose rate of more than 2–3% when techniques such as these are employed (70, 71).

We measured between 500 and 1000 individual quartz grains from each sample, and obtained between 97 and 183 independent estimates of $D_e$ from grains that passed all of the quality-assurance criteria (Table S8). About one-third of the grains in each of the Charnel House Cave samples, and 15–24% of measured grains in the Cathedral Cave samples, did not emit test-dose signals significantly above background ('$T_N$ signal <3xBG'). For the Charnel House Cave samples, a further 42–53% of measured grains were rejected either because their sensitivity-corrected regenerative-dose signals exhibited significant scatter between the duplicate doses ('Poor RR') or because the sensitivity-corrected natural signal was saturated or did not intercept the dose-response curve, or because the curve was hyperbolic in shape ('No $L_N/T_N$ intersection'). For the Cathedral Cave samples, 61–65% of measured grains were rejected on the basis of these two criteria. For all eight samples, a few grains were rejected because their OSL signals were reduced significantly after infrared stimulation ('Depletion by IR', which suggests the presence of feldspar inclusions) or because they suffered from significant recuperation ('0 Gy dose >5% $L_N/T_N$').

Most of the remaining grains (11–25% of the total measured) had signals characterised by a rapid decay of OSL with stimulation, which is indicative of them being dominated by the most light-sensitive ('fast') component of quartz OSL (a requirement for the reliable application of the SAR

procedure). The natural OSL decay curves of two individual grains of quartz from sample CHAR-2 are shown in Fig. S1, together with their dose-response curves (inset plots). The saturating exponential (a) and saturating exponential plus linear (b) growth curves are typical of those for other accepted grains from Charnel House Cave and Cathedral Cave, with the 'plus linear' function enabling finite $D_e$ values of several hundred Gy to be determined.

The $D_e$ distributions of all eight samples are displayed as radial plots (59, 76) in Fig. S2 (Charnel House Cave) and Fig. S3 (Cathedral Cave). Each point represents the $D_e$ value for a single grain, which can be read by drawing a line from the zero-point on the 'standardised estimate' axis (on the left), through the data point of interest, to intersect the $D_e$ axis (on the right). The uncertainty on this $D_e$ is obtained by drawing a vertical line from the data point to intersect the 'relative error' axis. The 'precision' is the reciprocal of the relative standard error, so $D_e$ values measured with the highest precision fall furthest to the right in radial plots. Furthermore, any shaded band of ± 2 units projecting from the standardised estimate axis will capture 95% of the points if they are statistically consistent at 2σ.

Clearly, no single shaded band can accommodate all of the $D_e$ estimates for any of the samples. The additional spread in $D_e$ can be quantified in terms of the 'overdispersion' (OD) value, which is the relative standard deviation of the $D_e$ estimates after their measurement errors have been taken into account (59, 76, 77). The $D_e$ distributions for all accepted grains have OD values of 31 ± 3 to 42 ± 4% (shown in regular type in Table S10 to distinguish them from the values highlighted in bold and in italics, which are discussed below). Such OD values lie at the upper end of the range reported for single-grain $D_e$ distributions of samples from the Jurreru River valley (56, 57) and for other samples that are known, or are thought, to have been fully bleached at burial and subsequently remained undisturbed and exposed to the same environmental dose rate (53, 78). Accordingly, the OD values of the Charnel House Cave and Cathedral Cave samples are consistent with the possibility that, in each sample, all of the grains were deposited at the same time, with natural variation in their OSL properties and environmental dose rates accounting for the overdispersion among the independent estimates of $D_e$. In such cases, the central age model (CAM) may be used to estimate the weighted

mean $D_e$ and its standard error, taking into account the measured OD (59, 76). The $D_e$ values calculated using the CAM are listed in Table S9 (in regular type), together with the OSL ages obtained by dividing these estimates by the corresponding total dose rates.

Some of the spread in $D_e$ values may, however, be due to insufficient sunlight exposure of some grains before deposition and/or to sediment mixing or substantial inhomogeneity in the beta dose rate to individual grains after deposition. The latter circumstance commonly applies when low-radioactivity materials (such as secondary carbonates) are precipitated between or around quartz grains (57, 63−67, 79) or when high-radioactivity materials (enriched in $^{40}K$, for example) occur in archaeological deposits (63, 64). The presence of spalled limestone debris in the Charnel House Cave and Cathedral Cave deposits raises the prospect that some quartz grains may have been surrounded or juxtaposed by finely disseminated carbonate, causing these grains to be exposed to greatly reduced beta dose rates and resulting, in turn, in correspondingly smaller $D_e$ values.

The presence of grains with atypically small $D_e$ values may also, or instead, reflect post-depositional intrusion of grains from younger (overlying) levels, while the small proportion of grains with unusually high $D_e$ values in each sample may represent intrusive grains from older (underlying) levels. However, we cannot discount the alternative possibility that the latter grains were incompletely bleached at the time of deposition. The existence of rubble layers in both cave sequences (Fig. 2) rules out the wholesale vertical displacement of grains, but the spatial distribution of volcanic glass shards at Charnel House Cave provides independent evidence for some post-depositional mixing. These microscopic shards, which Lane *et al*. (19) correlated with the Youngest Toba Tuff (YTT) based on their major element composition, form a non-visible 'cryptotephra' layer of highest concentration ~0.4 m below the top of the lower rubble layer and ~1 m above sample CHAR-4. But low concentrations of cryptotephra were also recorded in the overlying and underlying deposits, which Lane *et al*. (19) attributed to reworking of the glass shards and recent input from deflation of exposed YTT deposits in the surrounding landscape. The latter is unlikely to explain the traces of cryptotephra found beneath the main YTT layer, but some downward intrusion would be consistent with the presence in CHAR-4 of a few quartz grains with $D_e$ values as small as 40–50 Gy (Fig. S2). Post-

depositional mixing may also explain some of the spread in $D_e$ values for the three overlying CHAR samples.

To each of the $D_e$ distributions, we applied a statistical test based on the median absolute deviation, which is a robust scale estimator commonly used for outlier detection (80, 81). Some grains might have been incompletely bleached at the time of burial or were reworked subsequently, for example. The $D_e$ values of such grains should be removed from the data sets before calculating the weighted mean $D_e$ values and the corresponding OSL ages, to improve their accuracy. We converted the $D_e$ values (in Gy) to natural logarithms (following Galbraith and Roberts (76)) and rejected values with normalised median absolute deviations (nMADs, as defined by Powell *et al.* (80)) larger than 1.4826, which is the appropriate factor for a normal distribution, and with measurement uncertainties distinct from the median $D_e$ at 2σ. As single-grain $D_e$ values commonly vary widely in terms of their precision, the latter criterion avoids rejecting imprecise values with nMADs greater than 1.4826 but within statistical error of the median $D_e$. These outliers are displayed as open triangles in Figs. S2 and S3, with the remaining grains plotted as filled circles. The latter comprise the vast majority of accepted grains in each sample (87–91% and 92–97% of grains in the Charnel House Cave and Cathedral Cave samples, respectively) and have $D_e$ distributions with OD values of 16 ± 5 to 27 ± 4% (data highlighted in bold in Table S10). We consider the weighted mean $D_e$ values of these grains (estimated using the CAM) to be more accurate, as well as more precise, than those determined from the unfiltered $D_e$ data sets (i.e., before outlier rejection), but the two sets of estimates are indistinguishable at 2σ.

We also applied the finite mixture model (FMM) to the $D_e$ distributions of the Charnel House Cave and Cathedral Cave samples. The FMM can be used to determine the minimum number of discrete $D_e$ components needed to fit a single-grain distribution, the weighted mean $D_e$ values of those components and the proportion of grains in each component (62, 76, 77). We followed the procedures described in detail by David *et al*. (82) and Jacobs *et al*. (63, 66) to fit the FMM to each of the unfiltered $D_e$ data sets, using the Bayes Information Criterion and maximum log-likelihoods to determine the optimum fits. In each case, two or three components with OD values of 12–21% were

sufficient to fit the $D_e$ distributions, with the majority of grains contained in one of these components (data in italics in Table S9). The minor component(s) consisted of grains with $D_e$ values significantly larger or smaller than those included in the main component, and most of these grains were the same as those identified as outliers using the nMAD test.

As a consequence, the weighted mean $D_e$ values of the main FMM components are indistinguishable at 2σ from the CAM estimates of $D_e$ for the outlier-rejected data sets for all samples except CATH-2 and possibly CATH-3. The main $D_e$ components of CATH-2 and CATH-3 contain 72 and 60% of the total number of accepted grains, respectively, with the minor components consisting entirely of smaller $D_e$ values. We cannot plausibly explain 28–40% of these $D_e$ distributions in terms of downward displacement of younger grains, but these grains could conceivably have experienced substantially smaller beta dose rates from finely disseminated carbonate in the deposit, which is dominated by spalled limestone in this part of the sequence. We have, therefore, estimated the beta dose rates to the grains contained in the main $D_e$ components of CATH-2 and CATH-3 using the procedures described in detail elsewhere (64, 66, 79); the adjusted total dose rates are 1.35 ± 0.07 and 1.70 ± 0.08 Gy/ka, respectively.

We calculated the OSL age of each sample in three ways and these are listed in the final column of Table S10. To allow for any bias in the calibration of the laboratory beta source, a relative error of 2% is included in each of the age uncertainties. We first determined the age using the weighted mean $D_e$ estimate for all accepted grains (shown in regular type) and then calculated the age from the weighted mean $D_e$ of the grains remaining after rejecting the outliers (highlighted in bold). Finally, we obtained the ages using the weighted mean $D_e$ of the main FMM component of each single-grain distribution (listed in italics). As mentioned, the latter required a beta dose rate adjustment for CATH-2 and CATH-3 (asterisked in Table S9) because 28–40% of the grains were discarded, all with $D_e$ values smaller than the main component. Without this adjustment, the calculated ages increase to 188 ± 13 and 194 ± 19 ka, respectively; these ages are within statistical error of their beta-adjusted counterparts, but we consider them to be less accurate.

The three sets of OSL ages listed in Table S10 are indistinguishable at 2σ, demonstrating that the ages are insensitive to the inclusion or exclusion of outliers and are robust to a variety of reasonable and alternative assumptions. The concordance between the beta-adjusted ages for CATH-2 and CATH-3 and their CAM equivalents is typical of other samples to which this dose rate adjustment procedure has been applied (63−67). The ages highlighted in bold were determined after rejecting the most extreme $D_e$ values and are deemed to be the most reliable, as they make allowance for the possibility of insufficient sunlight exposure, post-depositional sediment mixing and/or greatly reduced beta dose rates affecting some (3–13%) of the grains.

Three features of the Charnel House Cave chronology are noteworthy. First, the ages are compatible with the stratigraphic positions of the OSL samples. The lower rubble layer, dated to 74.0 ± 4.4 ka, is significantly older than the overlying fine-grained 'cave earth' deposits, which have statistically consistent ages (55.9 ± 3.3 and 58.0 ± 3.1 ka) that give a weighted mean of 57.0 ± 2.6 ka. The upper rubble layer started to accumulate 58.3 ± 3.1 ka ago, soon after cessation of deposition of the cave earth, although the size of the uncertainties on these OSL ages could conceal a hiatus of a few centuries or, even, a few millennia. The second feature of interest is the possibility of a hiatus of 17 ± 4 ka between deposition of the lower rubble layer and the preserved cave earth deposits, if the uppermost ~1.4 m of rubble was deposited in its entirety ~74 ka ago. There remains the possibility, however, that it accumulated in discrete pulses, terminating shortly before ~57 ka; an age for the top of this rubble layer is needed to discriminate between these options.

The third noteworthy result at Charnel House Cave is the concordance between the OSL age for the lower rubble layer and the $^{40}Ar/^{39}Ar$ age of 73.88 ± 0.32 ka (83) or 75.0 ± 0.9 ka (84) for the YTT inferred from the chemical composition of the cryptotephra (19). This supports the proposition that the entire layer may have accumulated over a period of a few centuries, or less, ~74 ka ago, but we cannot resolve such short time intervals given the precision on the OSL age of a few millennia at 1σ. The OSL and cryptotephra data are also insufficient to falsify the alternative scenario of episodic accumulation of the rubble over a period of ~17 ka. The traces of cryptotephra recorded below the main YTT layer indicate either that the latter is *in situ* and some shards have infiltrated downwards

after deposition (19), or that the main YTT layer represents a secondary depositional event, with the shards reworked after 74 ka from a nearby source. Both possibilities are consistent with the $D_e$ distribution of sample CHAR-4, obtained for quartz grains only slightly larger than the glass shards (longest axis lengths of 50–150 μm). If the second scenario is correct, then the weighted mean OSL age of ~57 ka for the overlying cave earth provides a *terminus ante quem* for the time of reworking of the cryptotephra.

The OSL ages for the four Cathedral Cave samples are also in correct stratigraphic order, increasing from 122 ± 8 to 210 ± 15 ka over a depth interval of 3.6 m (Fig. 2). The two intervening OSL samples are separated vertically by ~70 cm of deposit containing large blocks of spalled limestone that could have accumulated rapidly. The statistically consistent ages of these samples (162 ± 11 and 164 ± 11 ka; weighted mean of 163 ± 9 ka) supports this suggestion, and implies that the deposits in both Charnel House Cave and Cathedral Cave accumulated in pulses, between about 210 and 57 ka ago.

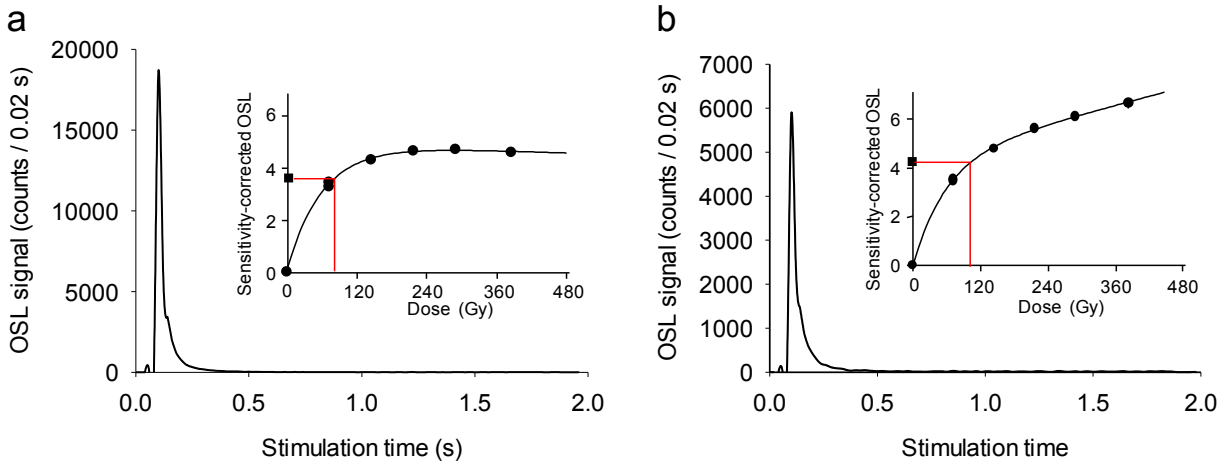


**Figure S1.** Natural OSL decay curves and dose-response curves (inset plots) for two individual grains of quartz from sample CHAR-2. The $D_e$ is estimated by projecting the sensitivity-corrected natural signal (shown by the filled square on the *y*-axis of each inset plot) on to the dose-response curve and reading the $D_e$ from the dose intercept on the *x*-axis. The $D_e$ values for these two grains are 83 ± 8 Gy (a) and 102 ± 11 Gy (b). The growth curves are fitted to 7 sensitivity-corrected regenerative-dose points (including a zero applied dose and a repeat measurement at a dose of 73 Gy) using a saturating exponential function (a) or a saturating exponential plus linear function (b).

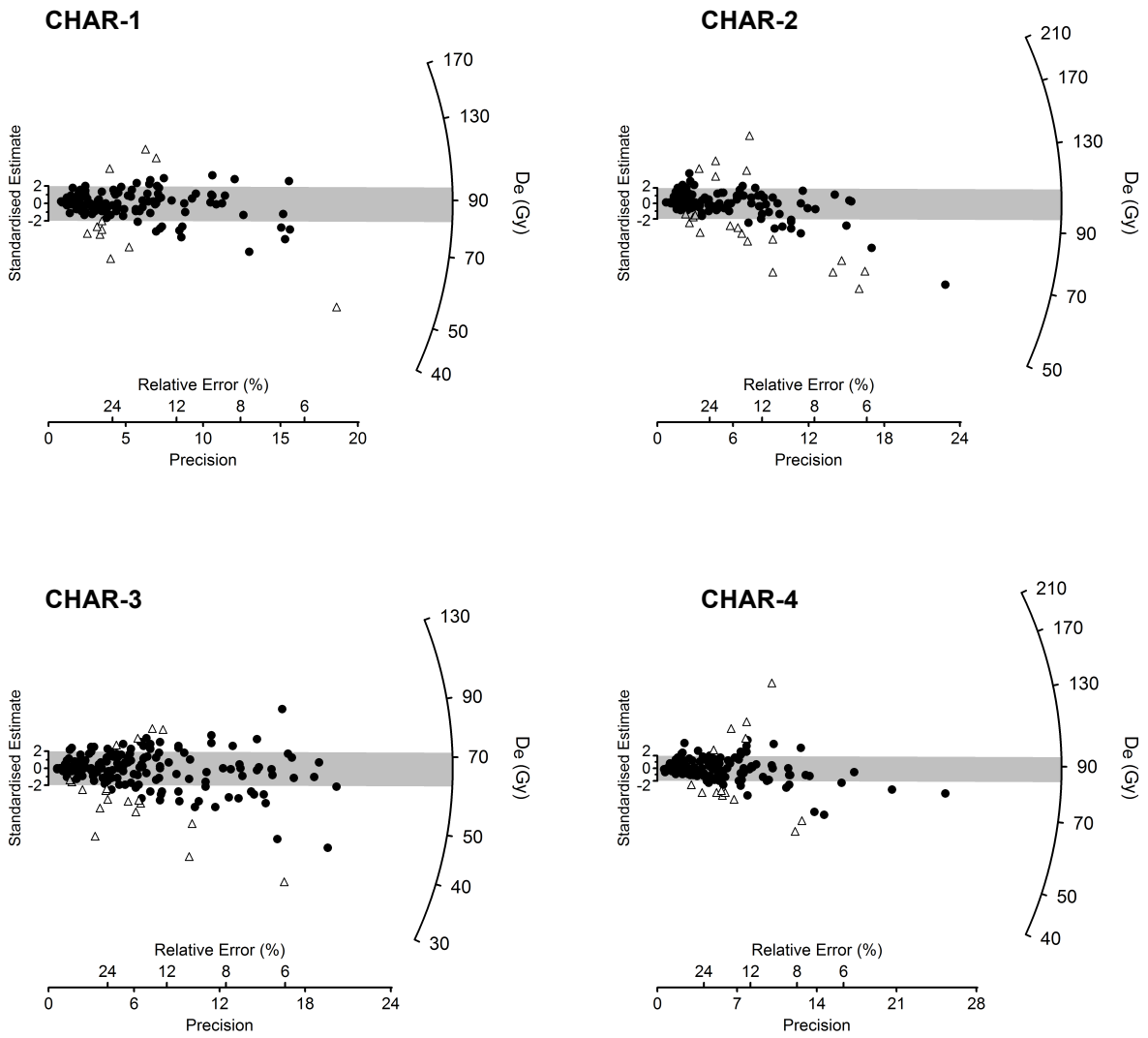


**Figure S2.** Radial plots of single-grain $D_e$ distributions for OSL samples from Charnel House Cave. If the $D_e$ estimates in each distribution were statistically consistent (at 2σ) with a common value, then 95% of the points should fall within any shaded band projecting ± 2 units from the standardised estimate axis. The $D_e$ values of all four samples are more dispersed than this (see text). The shaded band in each plot is centred on the weighted mean $D_e$ of the data points shown as filled circles, and these account for the vast majority (87–91%) of grains in each case (Table S9). The open triangles are $D_e$ values identified and rejected as statistical outliers.

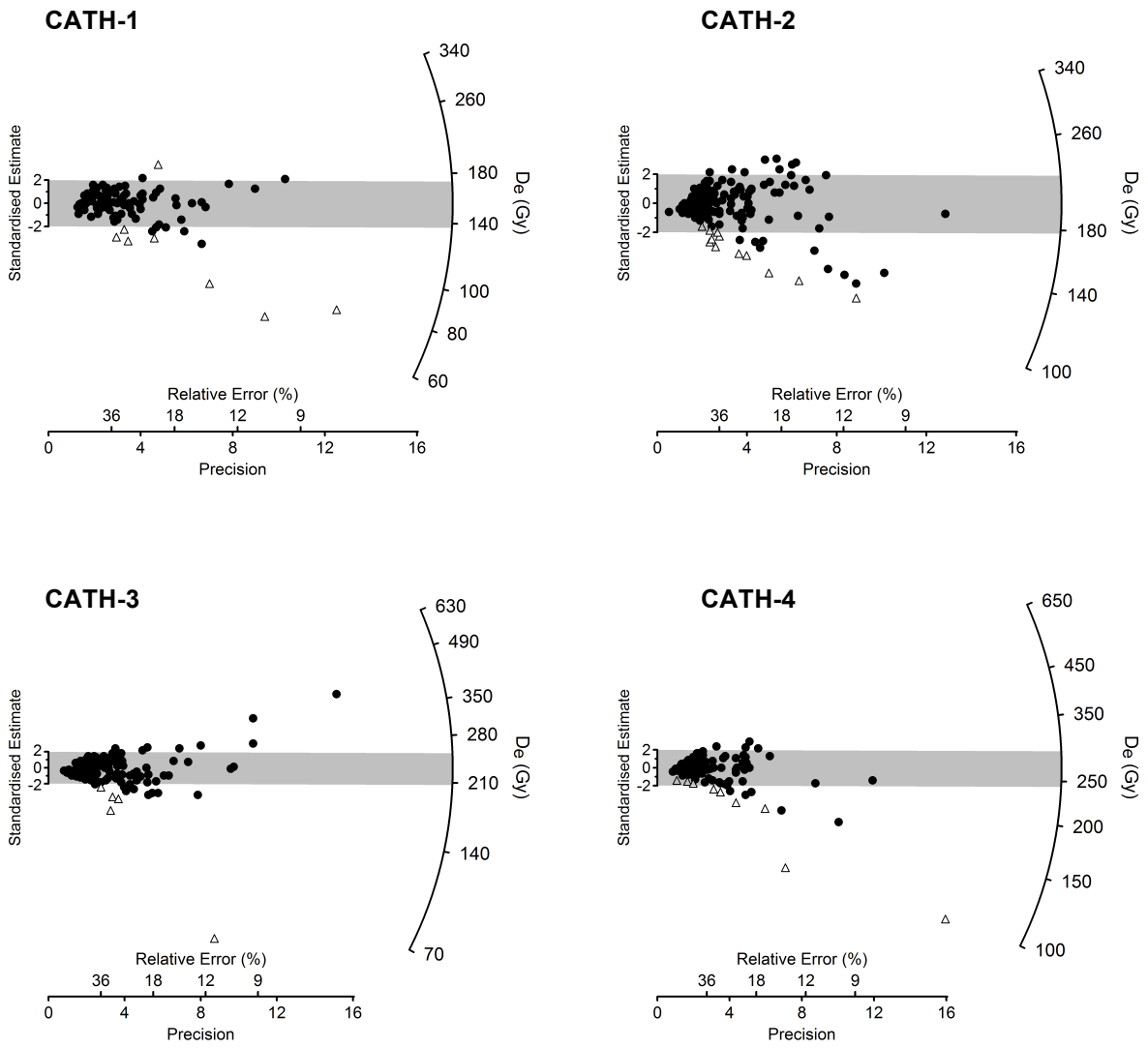


**Figure S3.** Radial plots of single-grain $D_e$ distributions for OSL samples from Cathedral Cave. See caption to Fig. S2 for explanation of symbols and shaded bands. For these samples, the $D_e$ values plotted as filled circles account for 92–97% of the grains (Table S9). CATH-3 has one extreme outlier with a $D_e$ of 20.4 ± 2.4 Gy, plotted as an open triangle.

**Table S1. List of the elements identified and their criteria for identification for each Genus/Species identified at Cathedral Cave.**

| Taxon | Elements identified/Criteria for identification |
|---|---|
| **Carnivora** | |
| *Ursus* sp. | Upper M3. L = 16.2, B = 10.5. Identified as 'Ursid'. |
| *Felis chaus* | Distal phalanx, right distal femur (BD = 15.8, DD =13.6) |
| *Panthera pardus* | Calcaneus (right, fragment) |
| *Herpestes griseus* | Upper P4 (left), humerus shaft (right). |
| *Canis* sp. | Metatarsal shaft near proximal end (probably wolf/wild dog). |
| *Vulpes* sp. | Metacarpal (distal end), lower P4 (right), |
| **Primates** | |
| *Semnopithecus entellus* | 08/3.1: Lower M1 or 2, rt, L=9.4, B=8.2<br>08/3.2: Lower dP4, rt, L=6.6, B=4.8<br>08/3.3: Molar frag<br>08/3.4: Upper molar frag<br>08/5.1: Lower right M1;<br>08/5.2: Lower right P4;<br>08/5.3: Upper left I1<br>08/5.4: Upper molar frag<br>08/5.5: Lower left P3<br>Left lower M2 (*Presbytis*?), left parietal (sutures open-juvenile), worn molar fragment, right ulna (cf. *Presbytis entellus*, very robust), small cranial vault fragment, parietal fragment |
| **Artiodactyla** | |
| *Bos* sp. | Upper dp4 (right), upper dp3 (right, worn), lower dp4 (left, at crown base L=31.3, B=12.9, at occlusal L=36.2, B=11.1, H=14.9 [on mesial]), lower M3 fragment |
| *Boselaphus* sp. | Molar fragment (x2), upper P4 (left), upper premolar, calcaneus (left), metacarpal III+IV (proximal, right) |
| *Antilope cervicapra* | Tarsal 2+3 (GL=15.7, GB=10.6), lower P3 (left, worn), proximal phalanx, (Right lateral/Left Medial, fused), upper M3 (very large, right, light wear), tooth fragment, middle phalanx (distal end, Bd=9.7); upper molar fragment, middle phalanx (Bp ca. 9.7, Bd=8.2, Dd=11.1), lower P4 (left, at base L=11.4, B=6.5, H=11.6 [at occlusal L=12.1, B=6.6]), lower M3 fragment, distal phalanx (Right lateral/Left Medial, very large - BP>11.3 [BP on comparative specimen is 9.5]). |
| *Gazella* sp. | Tooth fragments (x7) |
| Large bovid | Lower M3, lower I1, lower P2, lower di1, tooth fragments (x61) |
| Small bovid | Tooth fragment (*Gazella/Antelope*), molar fragment, middle phalanx (proximal end), lower I1 (left), tooth fragments (x2), femur shaft, metacarpal shaft, caudal vertebra, rib (proximal end), lower P4 (right), proximal phalanx (distal end), lower M2 fragment, |
| *Cervus* sp. | Lower dp3 (left, worn), upper molar fragments (x2) |
| *Cervus/Axis* | Tooth fragment, antler tine (tip) |
| *Axis axis* | Lower P3 (left, at crown base L=10.3, B=5.7, H=5.1 [heavy wear]), upper P3 (right, unworn), lower M1 (left), |

| | |
|---|---|
| *Muntjacus* sp. | Upper P4 (right, L = 8.7), upper C (right), |
| Small cervid | Upper M1 (right, very small, L = 6.8, B = 6.5) |
| *Sus* sp. | Lower I1 (left), lower canine fragments (right, male, very large [too large?], lower I1 (right, large individual), upper I1 (left), upper I2 (left), tooth fragments (x11), lower P4 (left, at base L=16.2, B=12.5 [at occlusal L=16.0], heavy wear), lower dp4 (right, very small, L = 11.8, B = 5.7), upper C (female), incisor, molar fragment, deciduous premolar fragment |
| **Other** | |
| *Equus* sp. | Upper premolar/molar (right), lower dp3-4 (left, at occlusal L=28.8, B=12.6, H=22.7), upper molar fragment (left, has long protocone), incisor fragments (x2), tooth fragments (may be from same tooth), premolar/molar fragment, incisor crown fragment |
| *Rhinoceros* sp. | Tooth fragments (x15), 2 lower premolar/molar fragments from 2 different teeth, 2 tooth fragments (thickness of enamel = 3.4 and 2.2 mm), tooth frag (enamel thickness=2.0 mm) |
| *Lepus* sp. | Metapodial (distal end), metacarpal shaft, proximal phalanx (distal end), maxilla fragment (right), innominate (left), |
| *Hystrix crassidens* | Upper P4 (right, unworn, L=9.6, B=6.0), upper M1 (right, worn, L=10.2, B=7.9), molar fragment, middle phalanx (hind foot, fused), lower P4 (right, L=9.6, B=5.5, light wear),<br>lower I1 fragment (B=8.65 - very large??), upper P4-M3 (left), metacarpal (distal end), incisor fragments (x2, very large individual)(B = 7.2 and B = 7.9), lower PM/M, 2 upper molars, upper incisor fragment (x2), tooth fragment (x10) |

**Table S2. List of the elements identified and their criteria for identification for each Genus/Species identified at Charnal House Cave.**

| **Taxon** | **Elements identified/Criteria for identification** |
|---|---|
| **Carnivora** | |
| *Herpestes griseus* | Acetabular portion of ischium and pubis (right) |
| **Primates** | |
| *Semnopithecus entellus* subsp. | Calcaneus (right) complete except for damage to the proximal end, astragalus (right, complete), metatarsal I (right, complete, with fused distal epiphysis), proximal pedal phalanx 1 (hindfoot, complete, GL=19.9mm, BP=10.2mm and BD=6.7mm), right proximal femur and shaft (50% fuysed femur present), right femur head (unfused with fovea), left proximal femur and shaft (75% of femur present), right tibia shaft (includes nutrient foramen, posterior surface, parts of anterior surface and parts of medial and lateral surfaces), right fibula shaft (five fragments, 75% of bone in total), caudal vertebrae (complete, fused centra on cranial and caudal ends), metapodial shaft fragment |
| **Artiodactyla** | |
| *Boselaphus* sp. | Lower M3 (right, fragment) |
| *Tetracerus* | Humerus (left, distal shaft fragment) |
| *Axis axis* | Lower molar (right, fragment) |
| **Other** | |
| *Equus* sp. | Lower cheek tooth (P3-M2, left) |
| *Rhinoceros* sp. | Rib shaft fragments (x2) (identified as 'most likely to be *Rhinoceros'* - comparison to comparative material at Deccan College shows them to be larger than *Buffalo* or *Bos*). |
| *Lepus* sp. | Maxilla (left), metatarsal IV (right, proximal end), mandible with P4 and M1 (right), metacarpal IV (left), premaxilla (right), metatarsal V (right, proximal end) |
| *Erinaceus* sp. | Tibia shaft (right) |

**Table S3. Total count of macrofauna identified to species and genera from Cathedral Cave, Billasurgam Cave complex. Fauna have been listed according to Marine Isotope Stages (MIS) as deduced from OSL dating through the sequence.**

| **Taxon** | **MIS 5** | **MIS 6** | **MIS 7** |
|---|---|---|---|
| *Rhinoceros* sp. | 18 | 2 | 0 |
| *Equus* sp. | 4 | 5 | 2 |
| *Bos* sp. | 2 | 2 | 0 |
| *Boselaphus* sp. | 2 | 4 | 1 |
| *Gazella* sp. | 3 | 3 | 1 |
| *Antilope cervicapra* | 2 | 9 | 0 |
| *Axis axis* | 3 | 0 | 0 |
| *Muntjacus* sp. | 0 | 2 | 0 |
| *Sus* sp. | 6 | 15 | 0 |
| *Lepus* sp. | 1 | 4 | 0 |
| *Hystrix crassidens* | 18 | 8 | 0 |
| *Semnopithecus entellus* | 11 | 4 | 1 |
| *Canis* sp. | 1 | 1 | 0 |
| *Vulpes* sp. | 1 | 1 | 0 |
| Ursid | 0 | 1 | 0 |
| *Felis chaus* | 0 | 2 | 0 |
| *Panthera pardus* | 1 | 0 | 0 |
| *Herpestes griseus* | 1 | 1 | 0 |
| *Erinaceus* sp. | 1 | 0 | 0 |
| **Total** | **75** | **64** | **5** |

**Table S4. Total count of macrofauna identified to species and genera from Charnel House Cave, Billasurgam Cave Complex. Fauna have been listed according to Marine Isotope Stages (MIS) as deduced from OSL dating through the sequence.**

| **Taxon** | **MIS 1/2** | **MIS 3** | **MIS 5** |
|---|---|---|---|
| *Rhinoceros* sp. | 0 | 1 | 1 |
| *Equus* sp. | 0 | 1 | 0 |
| *Boselaphus* sp. | 0 | 0 | 1 |
| *Tetracerus quadricornis* | 0 | 1 | 0 |
| *Axis axis* | 1 | 0 | 0 |
| *Lepus* sp. | 6 | 1 | 1 |
| *Hystrix crassidens* | 1 | 1 | 1 |
| *Semnopithecus entellus* | 0 | 0 | 18 |
| *Herpestes griseus* | 0 | 0 | 1 |
| *Erinaceus* sp. | 0 | 0 | 1 |
| **Total** | **8** | **5** | **24** |

**Table S5. Fauna identified by Lydekker (14) correlated with MIS periods inferred on the basis of SI Methods, Fi. 2, Table S6 and Table S7. N.B. As it has not been possible to re-identify these specimens they are not included in our total fauna counts and are used only for comparison. As a result, we also keep Lydekker's initial taxonomic nomenclature for these specimens (14). The specimen reidentified as *Theropithecus* in this paper (see Main Text and SI Methods) has been omitted from this table.**

| Taxa | MIS 1-5 | MIS 1/2 | MIS 5 | MIS 6 | MIS 6/7 |
|---|---|---|---|---|---|
| *Semnopithecus entellus* | + | + | + | | |
| *Felis tigris/leo* | | | | + | |
| *Hyaena crocuta* | + | | | + | |
| *Felis pardus* | + | | | | |
| *Felis chaus* | + | | | | |
| *Felis rubinginosa* | + | | | | |
| *Viverra karnuliensis* | | | + | | |
| *Prionodon* | + | | | | |
| *Herpestes griseus* | + | | | + | |
| *Herpestes fuscus* | + | | + | | |
| *Sorex* sp. | + | | | | |
| *Taphozous saccolemus* | + | | | | + |
| *Phylolorhina diadema* | + | | | + | |
| *Scius manus* | + | | | | |
| *Nesokia bandicoota* | + | | | + | |
| *Nesokia kok* | + | | | + | |
| *Hystrix crassidens* | + | | + | | |
| *Manis gigantea* | + | | | | |
| *Atherura karnuliensis* | | | + | | |

**Table S6a. Molar measurements (in mm) of *Theropithecus* samples from Billasurgam and elsewhere.**

| Taxon/population | N | LM1AW | LM1PW | LM1L | LM2AW | LM2PW | LM2L |
|---|---|---|---|---|---|---|---|
| GSI F-202, Charnel House Cave Bed M, MIS 5/6 (*T.* cf. *gelada*) | | | | | 8.35 | 8.43 | 11.82 |
| *Theropithecus gelada*, mean | 32-57 | 7.38 | 7.65 | 9.91 | 9.12 | 8.80 | 12.61 |
| maximum | | 8.02 | 8.70 | 11.12 | 10.40 | 9.83 | 14.50 |
| minimum | | 6.42 | 6.86 | 7.76 | 7.50 | 7.70 | 10.10 |
| *Theropithecus darti* (Hadar), mean | 16-19 | 8.33 | 8.11 | 10.54 | 10.22 | 9.68 | 12.88 |
| maximum | | 9.8 | 8.8 | 12.80 | 12.20 | 10.90 | 14.30 |
| minimum | | 7.3 | 7 | 8.50 | 8.70 | 8.40 | 11.20 |
| *Theropithecus oswaldi* cf. *oswaldi* (Konso, Matabaietu, Omo, Swartkrans), mean | 8-9 | 9.99 | 10.02 | 12.15 | 12.02 | 11.84 | 15.53 |
| maximum | | 12.40 | 11.40 | 14.10 | 32.80 | 32.87 | 17.00 |
| minimum | | 9.37 | 9.39 | 10.80 | 10.65 | 10.98 | 13.61 |
| | | UM2AW | UM2PW | UM2L | UM3AW | UM3PW | UM3L |
| *Theropithecus oswaldi oswaldi* (Konso, Koobi Fora, Matabaietu, Omo, Swartkrans), mean | 8-19 | 14.3 | 13.2 | 17.2 | 13.8 | 12.1 | 16.4 |
| maximum | | 16.5 | 16.4 | 20.9 | 15.0 | 13.8 | 18.8 |
| minimum | | 11.9 | 11.1 | 13.8 | 12.4 | 10.9 | 15.0 |
| *Theropithecus oswaldi leakeyi* (Konso, Middle Awash, Olorgesailie, Hopefield), mean | 5 (M2) 7(M3) | 17.1 | 15.9 | 19.9 | 16.3 | 14.1 | 20.7 |
| maximum | | 19.7 | 17.6 | 21.9 | 17.3 | 14.3 | 22.5 |
| minimum | | 15.6 | 13.7 | 18.5 | 15.6 | 13.6 | 19.5 |
| *Theropithecus oswaldi delsoni* (Mirzapur) | | 14.0 | 13.3 | 14.6 | 17.3 | 16.3 | 20.8 |

*Key: N, number of specimens for taxon (range); LM, lower molar; UM, upper molar; 1, 2, 3 molar position; AW, anterior width, maximum across the anterior (mesial) loph(id); PW, posterior width, maximum across the posterior (distal) loph(id); L, length, maximum mesiodistal.*

**Table S6b. Molar measurements (in mm) of *Semnopithecus entellus* (*S. e.*) samples from Billasurgam and elsewhere.**

| Taxon/population | N | UM1AW | UM1PW | UM1L | UM2AW | UM2PW | UM2L | UM3AW | UM3PW | UM3L |
|---|---|---|---|---|---|---|---|---|---|---|
| *S. e.* cf. *schistaceus* | | | | | | | | | | |
| female, GSI F-201, Charnel House Cave Bed A (MIS 1/2) | | 7.53 | 7.25 | 9.57 | 9.44 | 8.66 | 9.5 | 8.7 | 7.33 | 9.17 |
| *S. e.* cf. *schistaceus*/*ajax* | | | | | | | | | | |
| male, GSI F-201a, Charnel House Cave Bed M (MIS 5/6) | | 8.86 | 8.32 | 8.93 | 9.99 | 8.84 | 10.15 | | | |
| *S. e. schistaceus*, mean | 15-19 | 8.02 | 7.38 | 8.43 | 9.29 | 8.39 | 9.80 | 8.81 | 7.34 | 9.57 |
| maximum | | 8.73 | 8.12 | 9.18 | 10.23 | 9.10 | 10.69 | 10.08 | 7.90 | 10.59 |
| minimum | | 7.48 | 6.62 | 7.84 | 8.67 | 7.59 | 8.61 | 8.18 | 6.76 | 8.72 |
| *S. e. ajax*, mean | 3 | 8.19 | 7.32 | 8.48 | 9.67 | 8.66 | 9.95 | | | |
| maximum | | 8.5 | 7.7 | 8.7 | 10.1 | 8.8 | 10.1 | | | |
| *S. e.* cf. *entellus*, mean | 1-2 | 6.76 | 6.73 | 7.11 | 7.91 | 7.05 | 7.78 | 7.53 | 6.4 | 7.8 |
| *S. e. thersites*, mean | 22-24 | 6.21 | 5.99 | 6.66 | 7.06 | 6.47 | 7.22 | 6.73 | 5.79 | 7.10 |
| maximum | | 6.98 | 6.62 | 6.98 | 7.75 | 7.09 | 7.84 | 7.39 | 6.78 | 7.84 |
| minimum | | 5.49 | 5.13 | 6.20 | 6.40 | 5.62 | 6.61 | 6.10 | 4.62 | 6.45 |

| taxon/population | N | LM1AW | LM1PW | LM1L | LM2AW | LM2PW | LM2L | LM3AW | LM3PW | LM3L |
|---|---|---|---|---|---|---|---|---|---|---|
| *S. e.* cf. *schistaceus*/*ajax* | | 6.24 | 6.72 | 8.65 | 8.11 | 8.48 | 9.92 | 7.84 | 7.67 | 12.14 |

| | | | | | | | | | | |
|---|---|---|---|---|---|---|---|---|---|---|
| male, GSI F-201a, Charnel House Cave Bed M (MIS 5/6) | | | | | | | | | | |
| *S. e. schistaceus*, mean | 17-19 | 6.51 | 6.69 | 8.80 | 7.63 | 7.71 | 9.71 | 7.74 | 7.47 | 11.62 |
| maximum | | 6.82 | 7.21 | 9.48 | 8.44 | 8.44 | 10.58 | 8.52 | 8.28 | 12.85 |
| minimum | | 6.05 | 6.28 | 7.94 | 7.13 | 7.19 | 8.82 | 7.14 | 6.76 | 10.01 |
| *S. e. ajax*, mean | 3 | 6.87 | 7.22 | 8.97 | 8.21 | 8.28 | 9.89 | 8.44 | 7.89 | 12.43 |
| maximum | | 7.2 | 7.4 | 9.2 | 8.5 | 9.4 | 10.3 | 9.1 | 8.1 | 12.9 |
| *S. e.* cf. *entellus*, mean | 1-2 | 5.36 | 5.83 | 7.17 | 6.37 | 6.62 | 7.99 | 6.49 | 6.77 | 9.54 |
| *S. e. thersites*, mean | 24 | 5.08 | 5.31 | 6.86 | 6.04 | 6.05 | 7.34 | 6.03 | 5.84 | 9.02 |
| maximum | | 5.57 | 5.83 | 7.38 | 6.59 | 6.75 | 8.13 | 6.98 | 6.79 | 10.11 |
| minimum | | 4.58 | 4.86 | 6.39 | 5.49 | 5.56 | 6.73 | 5.47 | 5.10 | 8.11 |

*Key: N, number of specimens for taxon (range); LM, lower molar; UM, upper molar; 1, 2, 3 molar position; AW, anterior width, maximum across the anterior (mesial) loph(id); PW, posterior width, maximum across the posterior (distal) loph(id); L, length, maximum mesiodistal.*

*Comparative data were downloaded from PRIMO, the NYCEP PRImate Morphology Online database (http://primo.nycep.org).*

**Table S7. Correlation of 19th century stratigraphy (as per Foote, 1884) with modern excavations for Charnel House Cave. 19th century notes and descriptions come from Foote (13).**

| Foote's Bed designation | Foote's description | Thickness recorded by Foote (Feet, Inches) | Notes from 2003-2008 excavations | Estimated age given correlation with 2003-2008 excavations | Marine Isotope Stage |
|---|---|---|---|---|---|
| A1 | Surface (bat dung) bed | 3'-4' | Layers almost entirely removed by Foote. A thin remnant silty layer present containing charcoal and pottery (Foote notes potsherds in A1-C) | Holocene (pottery) | MIS 1/ MIS 2 |
| A | Rubble bed with large fallen blocks of limestone | 2'9" | | | |
| B, C | Stiff red clay with sandy partings | 3'6"-4' | | | |
| D, E | Rubble bed | 1'6"-2'6" | Pebble to boulder grade conglomerate, poorly sorted, well imbricated, dipping away from cave wall. Boulders are predominantly angular limestone whereas pebbles are a mixture of angular limestone and more rounded; other lithologies indicating moderate external sourcing of clasts. Intersecting ashy silt fills near top of unit. | 58 ± 3 ka (OSL) at base of section | MIS 3 |
| H | Red cave earth, stony above | 12" | Orange brown clay-rich silt (cave earth) | 58 ± 3 ka (OSL) top of section<br><br>56 ± 3 ka (OSL) base of section | MIS 3 |
| I | Red and mottled cave earth | 1'-1'3" | | | |
| J | Red-brown cave earth with patches of calcareous sand | 1' | | | |
| K,L | Red sandy cave earth with blocks of limestone | 1'6" | Coarse angular boulder rubble with beige brown cave earth matrix, clast supported, boulders dominated by weathered limestone roof rock (upper); zone of angular limestone cobbles strongly clast supported (middle); prominent concentration of large angular limestone boulders with fitted fabric (base) | Young Toba Tuff shards, *c.* 74 ka at top of section<br><br>74 ± 4 (OSL) in mid-section | MIS 5 |
| M,N | Stiff marly clay | 1' | Not excavated | Pre-74 ka | MIS 5 or earlier |

**Table S8. Correlation of 19th century stratigraphy with information from modern excavations for Cathedral Cave. 19th century notes and descriptions come from Foote (13).**

| Foote's Bed designation | Foote's description | Thickness recorded by Foote (Feet, Inches) | Notes from 2003-2008 excavations | Estimated age given correlation with 2003-2008 excavations | Marine Isotope Stage |
|---|---|---|---|---|---|
| C | Surface (bat's dung) turning to grey sandy with some bat's dung | 6' | Foote had cleared these layers (16 feet of sediment overall) from its entire surface, and his notes remain our only remaining record of these deposits. | Undated as layers were removed by Foote | - |
| Ca | Red sandy cave earth | 3' | | | |
| Cb, Cc | Stiff red clay excavated in three layers of 3' each | 6' | | | |
| Cd | Stiff red clay | 3' | Foote notes that the excavation of this layer exposed the mouth of the Corridor passage leading into the Fairy Chamber (see Fig. 1), into both of which the red clay extended and maintained its richness in fossil remains. Foote had removed half of this layer, while half remained to be excavated. This layer therefore matches the commencement of excavations in 2003-2008 (Haslam *et al.* 2010). | 122 ± 8 ka (OSL) mid-section | MIS 5 |
| Ce, Cf | Stiff dark marl | 6' | A similar stiff dark marl to Foote's excavation is found below the stiff red clay that represented the remains of bed Cd prior to excavation | 164 ± 11 ka (OSL) mid-section | MIS 6 |
| Ch | Dark loamy marl | 3' | Horizon cannot be identified in 2003-2008 excavations | | |
| Ci, Cj | Grey marl | 6' | These layers correspond to the more sterile material found at the base of the 2003-2008 excavation. | 162 ± 11 ka (OSL) top of section<br><br>210 ± 15 ka (OSL) mid-section | MIS 6/7 |
| Ck, Cl | Grey marl | 6' | | | |

**Table S9.** Number of grains measured, rejected and accepted, together with the reasons for their rejection [a]

| Sample | Grains measured | $T_N$ signal <3xBG | Poor RR | Depletion by IR | 0 Gy dose >5% $L_N/T_N$ | No $L_N/T_N$ intersection | Grains accepted | % accepted |
|---|---|---|---|---|---|---|---|---|
| CHAR-1 | 500 | 152 | 45 | 6 | 3 | 167 | 127 | **25.4** |
| CHAR-2 | 1000 | 301 | 183 | 14 | 4 | 343 | 155 | **15.5** |
| CHAR-3 | 800 | 254 | 211 | 6 | 6 | 140 | 183 | **22.9** |
| CHAR-4 | 800 | 272 | 140 | 12 | 3 | 227 | 146 | **18.3** |
| CATH-1 | 900 | 215 | 42 | 8 | 3 | 535 | 97 | **10.8** |
| CATH-2 | 1000 | 206 | 31 | 9 | 9 | 583 | 162 | **16.2** |
| CATH-3 | 900 | 136 | 57 | 10 | 3 | 530 | 164 | **18.2** |
| CATH-4 | 1000 | 243 | 42 | 16 | 5 | 568 | 126 | **12.6** |

[a] Grains were rejected as unsuitable if any of the following 5 criteria were applicable:

1. **$T_N$ signal <3xBG:** the initial OSL signal from the first test dose ($T_N$) was less than 3 times the background (BG) count rate.
2. **Poor RR:** the 'recycling ratio' between the sensitivity-corrected signals for duplicate regenerative doses was significantly (i.e., >2σ) different from unity.
3. **Depletion by IR:** the 'OSL IR depletion ratio' (58) was significantly (i.e., >2σ) smaller than unity.
4. **0 Gy dose >5% $L_N/T_N$:** the sensitivity-corrected signal measured in the 0 Gy regenerative-dose cycle was >5% of the sensitivity-corrected natural signal ($L_N/T_N$).
5. **No $L_N/T_N$ intersection:** $L_N/T_N$ was above or within the saturated region of the dose-response curve, or the dose-response curve followed a hyperbolic (rather than monotonic) function.

**Table S10.** Dose rate data, $D_e$ values and OSL ages for sediment samples from Charnel House Cave and Cathedral Cave (in stratigraphic order)

| Sample code [a] | Water [b] (%) | Dose rates [c] Beta (Gy/ka) | Gamma (Gy/ka) | Cosmic / Internal [d] (Gy/ka) | Total (Gy/ka) | Equivalent doses [e] Grains measured | Grains accepted | OD [f] (%) | $D_e$ [g] (Gy) | OSL age [h] (ka) |
|---|---|---|---|---|---|---|---|---|---|---|
| **Charnel House Cave** | | | | | | | | | | |
| CHAR-3 | 1.5 (5 ± 2) | 0.67 ± 0.04 | 0.42 ± 0.02 | 0.020 / 0.032 | 1.14 ± 0.05 | 800 | 183 | 35 ± 2 | 63.4 ± 2.0 | 55.5 ± 3.1 |
| | | | | | | | **164** | **23 ± 2** | **66.6 ± 1.6** | **58.3 ± 3.1** |
| | | | | | | | *97* | *13 (3)* | *60.9 ± 3.3* | *53.3 ± 3.8* |
| CHAR-2 | 14.2 (20 ± 3) | 1.09 ± 0.05 | 0.62 ± 0.04 | 0.017 / 0.032 | 1.76 ± 0.07 | 1000 | 155 | 35 ± 3 | 101.7 ± 3.7 | 58.0 ± 3.4 |
| | | | | | | | **135** | **17 ± 2** | **101.7 ± 2.6** | **58.0 ± 3.1** |
| | | | | | | | *119* | *15 (3)* | *102.5 ± 4.0* | *58.4 ± 3.5* |
| CHAR-1 | 19.7 (25 ± 4) | 1.11 ± 0.06 | 0.43 ± 0.03 | 0.015 / 0.032 | 1.59 ± 0.08 | 500 | 127 | 31 ± 3 | 86.6 ± 3.1 | 54.5 ± 3.5 |
| | | | | | | | **116** | **18 ± 2** | **88.8 ± 2.3** | **55.9 ± 3.3** |
| | | | | | | | *118* | *21 (3)* | *87.5 ± 3.1* | *55.1 ± 3.5* |
| CHAR-4 | 11.9 (15 ± 3) | 0.87 ± 0.05 | 0.29 ± 0.02 | 0.015 / 0.032 | 1.21 ± 0.06 | 800 | 146 | 36 ± 3 | 89.3 ± 3.3 | 74.0 ± 4.7 |
| | | | | | | | **132** | **22 ± 2** | **89.3 ± 2.5** | **74.0 ± 4.4** |
| | | | | | | | *118* | *21 (3)* | *91.3 ± 3.9* | *75.7 ± 5.1* |
| **Cathedral Cave** | | | | | | | | | | |
| CATH-1 | 10.9 (15 ± 3) | 0.76 ± 0.05 | 0.48 ± 0.03 | 0.004 / 0.032 | 1.27 ± 0.06 | 900 | 97 | 32 ± 4 | 145 ± 7 | 114 ± 8 |
| | | | | | | | **89** | **16 ± 5** | **155 ± 6** | **122 ± 8** |

| | | | | | | | | | | |
|---|---|---|---|---|---|---|---|---|---|---|
| | | | | | | | *84* | *16 (2)* | *162 ± 8* | *127 ± 9* |
| CATH-2 | 24.3 (25 ± 4) | 0.71 ± 0.05 | 0.47 ± 0.03 | 0.004 / 0.032 | 1.21 ± 0.06 | 1000 | 162 | 33 ± 4 | 185 ± 7 | 153 ± 10 |
| | | | | | | | **150** | **26 ± 4** | **200 ± 7** | **164 ± 11** |
| | | | | | | | *117* | *12 (2)* | *228 ± 9* | *169 ± 11** |
| CATH-3 | 21.3 (25 ± 4) | 0.80 ± 0.05 | 0.59 ± 0.04 | 0.004 / 0.032 | 1.43 ± 0.07 | 900 | 164 | 42 ± 4 | 217 ± 10 | 152 ± 11 |
| | | | | | | | **159** | **27 ± 4** | **231 ± 8** | **162 ± 11** |
| | | | | | | | *98* | *19 (3)* | *277 ± 22* | *163 ± 15** |
| CATH-4 | 22.0 (25 ± 4) | 0.65 ± 0.04 | 0.59 ± 0.04 | 0.004 / 0.032 | 1.28 ± 0.06 | 1000 | 126 | 37 ± 5 | 248 ± 12 | 194 ± 14 |
| | | | | | | | **117** | **25 ± 5** | **268 ± 11** | **210 ± 15** |
| | | | | | | | *103* | *18 (3)* | *289 ± 15* | *226 ± 17* |

[a] Individual quartz grains of 180–212 μm diameter were measured for all samples.

[b] Measured (field) water contents (mass of water expressed as % mass of dry sample) and, in parentheses, the long-term values used for dose rate and age determinations. Uncertainties were assigned to accommodate (at 2σ) the field values and any likely variations integrated over the period of sample burial.

[c] Mean ± total (1σ) uncertainty, calculated as the quadratic sum of the random and systematic errors. The beta dose rate uncertainty includes two systematic errors (each of 3%) to allow for possible bias in the beta-dose attenuation factors and the beta-counting laboratory standard.

[d] Cosmic-ray and internal alpha dose rates were assigned relative standard errors of 10% and 30%, respectively.

[e] Data in regular type refer to grains with OSL properties that met all quality-assurance criteria and for which equivalent dose ($D_e$) values were obtained. Data highlighted in bold refer to the same grains after additionally rejecting $D_e$ values with normalised median absolute deviations >1.4826 and measurement uncertainties distinct from the median $D_e$ at 2σ. Data in italics refer to the grains contained in the main component of the $D_e$ distributions fitted using the finite mixture model (FMM).

[f] Overdispersion (OD), the relative spread in the $D_e$ distributions beyond that associated with the individual measurement uncertainties. Values in italics are the OD values (and, in parentheses, the number of components) used to obtain optimum fits with the FMM.

[g] Values in regular type and in bold are the central age model (CAM) estimates of the weighted mean $D_e$ and standard error for all accepted grains, taking into account the extent of overdispersion. Values in italics are the CAM estimates of the weighted mean $D_e$ and standard error for the grains contained in the main component identified by the FMM.

[h] Mean ± total (1σ) uncertainty, calculated as the quadratic sum of the random and systematic errors. The total uncertainty includes all measurement uncertainties, the overdispersion among $D_e$ values and a relative error of 2% to allow for possible bias in calibration of the laboratory beta source. The two ages marked with an asterisk were calculated using adjusted beta dose rates (see text for discussion and adjusted values). The ages highlighted in bold are considered more accurate than those shown in regular type or in italics, as explained in the text.

**Table S11.** Beta dose rates determined by high-resolution gamma-ray spectrometry (HRGS) and GM-25-5 beta counting [a]

| Radionuclide activities (Bq/kg) | Sample CHAR-1 | Sample CHAR-2 |
|---|---|---|
| $^{238}$U | 19.15 ± 1.55 | 18.23 ± 1.32 |
| $^{226}$Ra | 23.21 ± 0.38 | 21.24 ± 0.33 |
| $^{210}$Pb | 22.48 ± 1.76 | 17.12 ± 1.11 |
| $^{228}$Ra | 44.21 ± 0.86 | 41.85 ± 0.73 |
| $^{228}$Th | 43.71 ± 0.83 | 40.48 ± 0.73 |
| $^{40}$K | 430 ± 10 | 397 ± 9 |
| HRGS beta dose rate (Gy/ka) | 1.46 ± 0.03 | 1.33 ± 0.03 |
| GM-25-5 beta dose rate (Gy/ka) | 1.39 ± 0.05 | 1.40 ± 0.05 |
| HRGS / GM-25-5 beta dose rates | 1.05 ± 0.04 | 0.95 ± 0.04 |

[a] Dry and attenuated beta dose rates. The uncertainties reflect the propagated random errors at 1σ.

**Supporting Information References**


47. Szalay FS, Delson E (1979) *Evolutionary History of the Primates* (Academic Press, New York).

48. Belay G, Mori A (2006) Intraspecific phylogeographic mitochondrial DNA (D-loop) variation of Gelada baboon, *Theropithecus gelada*, in Ethiopia. *Biochem Syst Ecol* 34: 554–561.

49. Delson E, et al. (2000) *Body Mass in Cercopithecidae (Primates, Mammalia): Estimation and Scaling in Extinct and Extant Taxa* (American Museum of Natural History, New York, Anthropological Paper 83).

50. Huntley DJ, Godfrey-Smith DI, Thewalt MLW (1985) Optical dating of sediments. *Nature* 313**:**105–107.

51. Aitken MJ (1998) *An Introduction to Optical Dating* (Oxford University Press, Oxford).

52. Lian OB, Roberts RG (2006) Dating the Quaternary: progress in luminescence dating of sediments. *Quat Sci Rev* 25: 2449–2468.

53. Jacobs Z, Roberts RG (2007) Advances in optically stimulated luminescence dating of individual grains of quartz from archeological deposits. *Evol Anthropol* 16: 210–223.

54. Duller GAT (2008) Single-grain optical dating of Quaternary sediments: why aliquot size matters in luminescence dating. *Boreas* 37: 589–612.

55. Wintle AG (1997) Luminescence dating: laboratory procedures and protocols. *Radiat Meas* **27**, 769–817.

56. Petraglia M, et al. (2007) Middle Paleolithic assemblages from the Indian subcontinent before and after the Toba super-eruption. *Science* 317: 114–116.

57. Haslam M, et al. (2012) A southern Indian Middle Palaeolithic occupation surface sealed by the 74 ka Toba eruption: further evidence from Jwalapuram Locality 22. *Quat Internat* 258: 148–164.

58. Murray AS, Roberts RG (1998). Measurement of the equivalent dose in quartz using a regenerative-dose single-aliquot protocol. *Radiat Meas* 29: 503–515.

59. Galbraith RF, et al. (1999) Optical dating of single and multiple grains of quartz from Jinmium rock shelter, northern Australia: Part I, experimental design and statistical models. *Archaeometry* 41: 339–364.

60. Jacobs Z, Duller GAT, Wintle AG (2006) Interpretation of single grain $D_e$ distributions and calculation of $D_e$. *Radiat Meas* 41: 264–277.

61. Jacobs Z, Duller GAT, Wintle AG (2003) Optical dating of dune sand from Blombos Cave, South Africa: II—single grain data. *J Hum Evol* 44: 613–625.

62. Jacobs Z, Duller GAT, Wintle AG, Henshilwood CS (2006) Extending the chronology of deposits at Blombos Cave, South Africa, back to 140 ka using optical dating of single and multiple grains of quartz. *J Hum Evol* 51: 255–273.

63. Jacobs Z, Wintle AG, Duller GAT, Roberts RG, Wadley L (2008) New ages for the post-Howiesons Poort, late and final Middle Stone Age at Sibudu, South Africa. *J Archaeol Sci* 35: 1790–1807.

64. Jacobs Z, Wintle AG, Roberts RG, Duller GAT (2008) Equivalent dose distributions from single grains of quartz at Sibudu, South Africa: context, causes

and consequences for optical dating of archaeological deposits. *J Archaeol Sci* 35: 1808–1820.

65. Jacobs Z, et al. (2008) Ages for the Middle Stone Age of southern Africa: implications for human behavior and dispersal. *Science* 322: 733–735.

66. Jacobs Z, et al. (2011) Single-grain OSL dating at La Grotte des Contrebandiers ('Smugglers'Cave'), Morocco: improved age constraints for the Middle Palaeolithic levels. *J Archaeol Sci* 38: 3631–3643.

67. Jacobs Z, Hayes EH, Roberts RG, Galbraith RF, Henshilwood CS (2013) An improved OSL chronology for the Still Bay layers at Blombos Cave, South Africa: further tests of single-grain dating procedures and a re-evaluation of the timing of the Still Bay industry across southern Africa. *J Archaeol Sci* 40: 579–594.

68. Roberts RG, Galbraith RF, Olley JM, Yoshida H, Laslett GM (1999) Optical dating of single and multiple grains of quartz from Jinmium rock shelter, northern Australia: Part II, results and implications. *Archaeometry* 41: 365–395.

69. Bøtter-Jensen L, Mejdahl V (1988) Assessment of beta dose-rate using a GM multicounter system. *Nucl Tracks Radiat Meas* 14: 187–191.

70. Olley JM, Murray A, Roberts RG (1996) The effects of disequilibria in the uranium and thorium decay chains on burial dose rates in fluvial sediments. *Quat Sci Rev* 15: 751–760.

71. Olley JM, Roberts RG, Murray AS (1997) Disequilibria in the uranium decay series in sedimentary deposits at Allen's Cave, Nullarbor Plain, Australia: implications for dose rate determinations. *Radiat Meas* 27: 433–443.

72. Prescott JR, Hutton JT (1994) Cosmic ray contributions to dose rates for luminescence and ESR dating: large depths and long-term time variations. *Radiat Meas* 234: 497–500.

73. Turney CSM, et al. (2001) Early human occupation at Devil's Lair, southwestern Australia 50,000 years ago. *Quat Res* 55: 3–13.

74. Prideaux GJ, et al. (2007) Mammalian responses to Pleistocene climate change in southeastern Australia. *Geology* 35: 33–36.

75. Roberts RG, et al. (2009) Geochronology of cave deposits at Liang Bua and of adjacent river terraces in the Wae Racang valley, western Flores, Indonesia: a synthesis of age estimates for the type locality of *Homo floresiensis*. *J Hum Evol* 57: 484–502.

76. Galbraith RF, Roberts RG (2012) Statistical aspects of equivalent dose and error calculation and display in OSL dating: an overview and some recommendations. *Quat Geochron* 11: 1–27.

77. Roberts RG, Galbraith RF, Yoshida H, Laslett GM, Olley JM (2000) Distinguishing dose populations in sediment mixtures: a test of single-grain optical dating procedures using mixtures of laboratory-dosed quartz. *Radiat Meas* 32: 459–465.

78. Arnold LJ, Roberts RG (2009) Stochastic modelling of multi-grain equivalent dose ($D_e$) distributions: implications for OSL dating of sediment mixtures. *Quat Geochron* 4: 204–230.

79. Haslam M, et al. (2011) Late Acheulean hominins at the Marine Isotope Stage 6/5e transition in north-central India. *Quat Res* 75: 670–682.

80. Powell R, Hergt J, Woodhead J (2002) Improving isochron calculations with robust statistics and the bootstrap. *Chem Geol* 185: 191–204.

81. Rousseeuw PJ, Debruyne M, Engelen S, Hubert M (2006) Robustness and outlier detection in chemometrics. *Crit Rev Anal Chem* 36: 221–242.

82. David B, et al. (2007) Sediment mixing at Nonda Rock: investigations of stratigraphic integrity at an early archaeological site in northern Australia and implications for the human colonisation of the continent. *J Quat Sci* 22: 449–479.

83. Storey M, Roberts RG, Saidin M (2012) Astronomically calibrated $^{40}Ar/^{39}Ar$ age for the Toba supereruption and global synchronization of late Quaternary records. *Proc Natl Acad Sci USA* 109: 18684–18688.

84. Mark DF, et al. (2013) A high-precision $^{40}Ar/^{39}Ar$ age for the Young Toba Tuff and dating of ultra-distal tephra: forcing of Quaternary climate and implications for hominin occupation of India. *Quat Geochron* http://dx.doi.org/10.1016/